NAVAL POSTGRADUATE SCHOOL
Monterey, California

THESIS

CONTINUED INVESTIGATION OF THE USE OF PASSIVE RESONATORS TO IMPROVE THE PERFORMANCE OF A LOW FREQUENCY SONAR TRANSDUCER

by

David E. Sanders

December, 1991

Thesis Advisor: S.R. Baker
Second Reader: O.B. Wilson

Approved for public release; distribution is unlimited.

REPORT DOCUMENTATION PAGE

Form Approved OMB No. 0704-0188

1a REPORT SECURITY CLASSIFICATION: Unclassified	1b RESTRICTIVE MARKINGS
2a SECURITY CLASSIFICATION AUTHORITY	3 DISTRIBUTION / AVAILABILITY OF REPORT: Approved for public release; distribution is unlimited.
2b DECLASSIFICATION / DOWNGRADING SCHEDULE	
4 PERFORMING ORGANIZATION REPORT NUMBER(S)	5 MONITORING ORGANIZATION REPORT NUMBER(S)
6a NAME OF PERFORMING ORGANIZATION: Naval Postgraduate School; 6b OFFICE SYMBOL (If applicable): 33	7a NAME OF MONITORING ORGANIZATION: Naval Postgraduate School
6c ADDRESS (City, State, and ZIP Code): Monterey, CA 93943-5000	7b ADDRESS (City, State, and ZIP Code): Monterey, CA 93943-5000
8a NAME OF FUNDING / SPONSORING ORGANIZATION; 8b OFFICE SYMBOL (If applicable)	9 PROCUREMENT INSTRUMENT IDENTIFICATION NUMBER
8c ADDRESS (City, State, and ZIP Code)	10 SOURCE OF FUNDING NUMBERS: PROGRAM ELEMENT NO; PROJECT NO; TASK NO; WORK UNIT ACCESSION NO

11 TITLE (Include Security Classification)
Continued Investigation Of The Use Of Passive Resonators To Improve The Performance Of A Low Frequency Sonar Transducer

12 PERSONAL AUTHOR(S)
Sanders, David E.

13a TYPE OF REPORT	13b TIME COVERED	14 DATE OF REPORT (Year, Month, Day)	15 PAGE COUNT
Master's Thesis	FROM _____ TO _____	1991 December	84

16 SUPPLEMENTARY NOTATION The views expressed in this thesis are those of the author and do not reflect the official policy or position of the Department of Defense or the U.S. Government.

17 COSATI CODES			18 SUBJECT TERMS (Continue on reverse if necessary and identify by block number)
FIELD	GROUP	SUB-GROUP	Low Frequency Active, Coupled Network Analysis, Passive Acoustic Resonators

19 ABSTRACT (Continue on reverse if necessary and identify by block number)

In an earlier thesis, Ellsworth showed that the radiated power output (quantified by the gain in radiation resistance presented to the transducer) and directivity of a compact underwater transducer can be significantly improved by the use of a system of resonant scatterers. These resonant scatterers were termed "sympathetic resonators". In the present work, we verify the previous findings and extend the work to additional cases of interest. Specifically, we (1) employ equations requiring fewer assumptions and implement them using more

20 DISTRIBUTION / AVAILABILITY OF ABSTRACT	21 ABSTRACT SECURITY CLASSIFICATION	
☒ UNCLASSIFIED/UNLIMITED ☐ SAME AS RPT ☐ DTIC USERS		
22a NAME OF RESPONSIBLE INDIVIDUAL: Steven R. Baker	22b TELEPHONE (Include Area Code): (408) 646-2732	22c OFFICE SYMBOL: PH/BA

DD Form 1473, JUN 86 — Previous editions are obsolete. S/N 0102-LF-014-6603

accurate numerical techniques, (2) reproduce Ellsworth's calculations and provide graphical results for conical and planar circular configurations for the case of six passive acoustic resonators, (3) extend the theory to and provide results for two types of linear arrays of passive acoustic resonators, (4) and finally, we consider an acoustic Yagi-Uda antenna-like configuration of passive acoustic resonators to improve the directivity of an underwater transducer. The results indicate that the conical configuration of six resonators is the best choice in terms of the gain in radiated power output, directivity along an acoustic axis, and minimum required number of resonators.

Approved for public release; distribution is unlimited.

Continued Investigation Of The Use Of Passive Resonators To Improve The Performance Of A Low Frequency Sonar Transducer

by

David E. Sanders
Lieutenant, United States Navy
B.S.E.E., North Carolina State University, 1985

Submitted in partial fulfillment
of the requirements for the degree of

MASTER OF SCIENCE IN ENGINEERING ACOUSTICS
and
MASTER OF SCIENCE IN APPLIED SCIENCE
(Antisubmarine Warfare)

from the
NAVAL POSTGRADUATE SCHOOL
December 1991

Author: David E. Sanders

Approved by: Steven R. Baker, Thesis Advisor

Oscar B. Wilson, Second Reader

Anthony A. Atchley, Chairman
Engineering Acoustics Academic Committee

James N. Eagle, Chairman
Antisubmarine Warfare Academic Group

ABSTRACT

In an earlier thesis, Ellsworth showed that the radiated power output (quantified by the gain in radiation resistance presented to the transducer) and directivity of a compact underwater transducer can be significantly improved by the use of a system of resonant scatterers. These resonant scatterers were termed "sympathetic resonators." In the present work, we verify the previous findings and extend the work to additional cases of interest. Specifically, we (1) employ equations requiring fewer assumptions and implement them using more accurate numerical techniques, (2) reproduce Ellsworth's calculations and provide graphical results for conical and planar circular configurations for the case of six passive acoustic resonators, (3) extend the theory to and provide results for two types of linear arrays of passive acoustic resonators, (4) and finally, we consider an acoustic Yagi-Uda antenna-like configuration of passive acoustic resonators to improve the directivity of an underwater transducer. The results indicate that the conical configuration of six resonators is the best choice in terms of the gain in radiated power output, directivity along an acoustic axis, and minimum required number of resonators.

TABLE OF CONTENTS

ACKNOWLEDGEMENTS

I would like to thank my loving wife, Kari, for her support during my work on this thesis. Words cannot express my appreciation enough. I would also like to thank Professor Steve Baker for his time, efforts, and guidance in this research. Thanks to Professor O. B. Wilson for his support and resources. Thanks to Professors Colson and Blau for their assistance in using the SUN workstation computers in support of this research.

LIST OF SYMBOLS

a_n	radius of element n
BP	beam pattern
c	sound speed
d_m	distance from resonator m to the transducer in Yagi-Uda configuration
D_n	diffraction constant of element n
f	force of fluid on transducer surface
$Gain$	gain in radiation resistance
H	height of transducer above the plane of resonators in conical configuration
I_0	current through the electrical terminals of the transducer
k	wavenumber
ka	wavenumber times the radius of resonator
ka_r	value of ka at resonance of a single bubble
ka_0	wavenumber times radius of transducer
l	distance between adjacent elements in line arrays
l_{nm}	distance from element n to element m
L	distance from transducer to first resonator in line arrays
m_r	radiation mass
N	number of resonators
p_n	acoustic pressure at the surface of element n

p_n^b	blocked acoustic pressure at element n
p_n^{ff}	free-field pressure at element n
p_n^{field}	acoustic pressure at a field point due to element n
p_{tot}^{field}	acoustic pressure at a field point due to all elements
p_n^{rad}	surface acoustic pressure radiated by element n
p_{ax}	acoustic pressure along an acoustic axis
P_0	hydrostatic pressure
p_s	acoustic pressure due to a spherical source
r_n	distance to field point from element n
R	radius of a circle of resonators
R_r	radiation resistance
s	mechanical stiffness of a bubble
S	surface area of a bubble
T	transduction coefficient
T_0	period of harmonic motion
u	particle velocity
U_n	acoustic volume velocity of resonator n
U_0	acoustic volume velocity of transducer
U^{rel}	relative volume velocity, $U^{rel} = U_n/U_0$
V_0	voltage across the electrical terminals of the transducer
Z_n^a	acoustic impedance of element n

Z^{ao}	open circuit acoustic impedance of the transducer
Z^{ar}_{nn}	acoustic radiation impedance presented to element n with all other elements blocked
Z^{ar}_{nm}	acoustic transfer impedance from element m to element n
Z^{ar}_{total}	total acoustic radiation impedance seen by the transducer in the presence of passive acoustic radiators
Z^{arf}_{nm}	free-field acoustic transfer impedance from element m to element n
Z^{EB}	blocked electrical impedance of the transducer
γ	ratio of specific heats, $\gamma = 1.4$ for air
δ_{nm}	Kronecker delta function
θ	polar angle in spherical coordinates
λ	wavelength
$\prod_N$	power radiated by a transducer with N passive acoustic resonators
ϕ	azimuthal angle in spherical coordinates
ω	angular frequency
ω_0	resonant angular frequency
$\{X\}$	a 1xN column matrix
$[X]$	a NxN square matrix

I. INTRODUCTION

A. BACKGROUND

It has been shown that a coupled set of resonant scatterers will, at frequencies near the resonance of a single scatterer, exhibit a quasiresonant condition, resulting in a significantly higher scattering cross section than a single scatterer [Ref. 1], [Ref. 2]. This phenomena has been shown by I. Tolstoy to provide significant gain in the scattered acoustic pressure to a plane wave when incident upon a system of scatterers as in Figure 1-1 [Ref. 3]. Tolstoy demonstrated that, particularly for the line array, the amplification

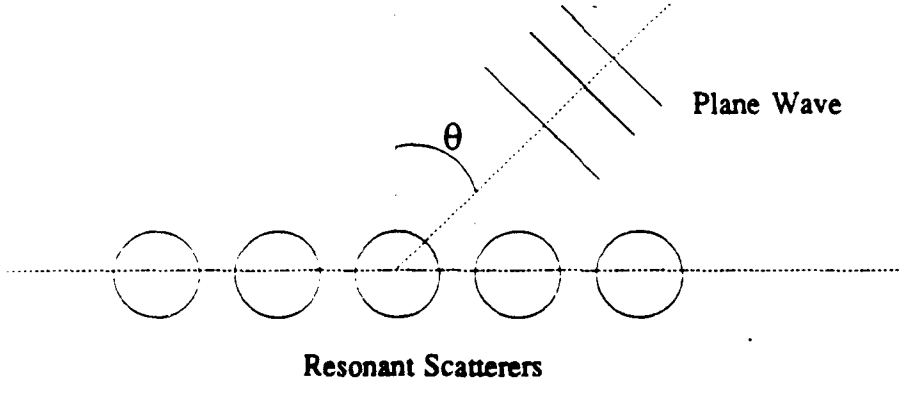

Figure 1-1 Plane wave incident upon a system of resonant scatterers.

of the scattered wave is sensitive to the direction of the incoming plane wave [Ref. 3]. In his thesis [Ref. 4], J. Ellsworth considered the effect of the presence of a system of resonant acoustic scatterers on a transducer in the coupled acoustic field as in Figure 1-2.

Ellsworth referred to these resonant scatterers as "sympathetic resonators." We will refer to these scatterers as passive acoustic resonators. Two geometries were previously considered. The first, called the planar configuration, placed the transducer in the center of a circular array of resonators. The second, called the conical configuration, is the

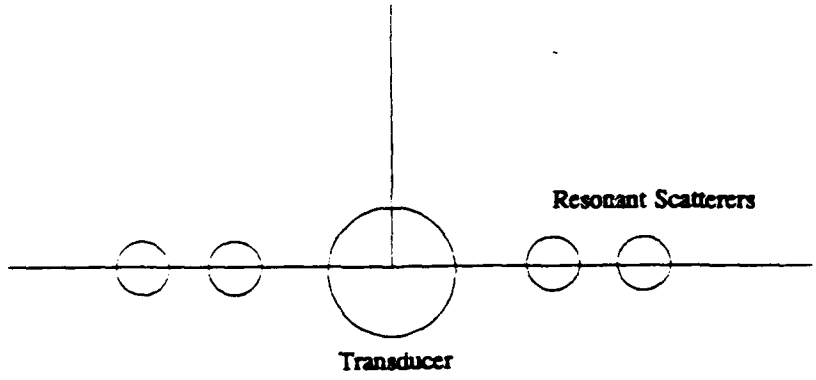

Figure 1-2 A transducer in a coupled field of resonators.

same as the planar configuration except that the transducer is displaced one-quarter wavelength out of the plane of the resonators. The results demonstrated a gain in radiation resistance presented to the transducer. This means that, for a displacement limited transducer, more power can be radiated into the medium. Ellsworth also provided beam patterns demonstrating that the transducer will, in the presence of passive acoustic resonators, exhibit directionality along an acoustic axis.

B. OBJECTIVES

The objectives of this thesis are to (1) refine the theory presented by Ellsworth using equations requiring fewer assumptions and implementing those equations with more accurate numerical methods, (2) reproduce Ellworth's work using the more accurate

techniques and provide three-dimensional plots for the case of six resonators (the six resonator results were requested by the Naval Ocean Systems Center), (3) develop three dimensional beam patterns for all cases of interest, (4) develop the theory for and provide results for two types of line arrays of passive acoustic resonators, and (5) to consider an acoustic Yagi-Uda [Ref. 5] antenna-like configuration of scatterers to improve the directivity of an underwater transducer.

Our measures of effectiveness in the above work will be (1) the gain in radiation resistance presented to the transducer with the system of passive acoustic radiators present, (2) three-dimensional plots of that gain versus the system parameters, (3) the directivity index of the transducer in the presence of passive acoustic radiators, and (4) the shape of and characteristics of the far-field beam pattern for each configuration considered. In support of these objectives, programs were written in *Mathematica* [Ref. 6] (a system for doing mathematics by computer) on Macintosh, IBM, and SUN workstation computers. An example program is provided in the appendix.

The remainder of this thesis is organized as follows. We first develop the theory for a transducer in a coupled acoustic field with passive acoustic resonators. We provide results for the two circular configurations, planar and conical. We analyze and provide results for two types of line arrays of resonators, termed line type I and line type II. We consider the acoustic Yagi-Uda array of resonators. Finally, we discuss the results and provide conclusions and recommendations.

II. THEORY

A. THE NETWORK MODEL

We will develop the network model for a coupled network of a transducer and N passive acoustic resonators by considering each element as a lumped acoustic system. The development is similar to that presented by Ellsworth [Ref. 4]. We will represent each lumped acoustic element as an acoustic impedance, choosing pressure and volume velocity as mechanical variables. In Section 1 we develop the network representation of a single resonator in an acoustic field. In Section 2 we develop the network representation of a transducer in an acoustic field. In Section 3 we combine the results of Sections 1 and 2, and develop a network model for a transducer coupled to N resonators by an acoustic field. We allow for interactions between each element and every other element. This network will be used to analyze systems of passive acoustic resonators in the chapters that follow. Finally, in Section 4, we discuss the required input parameters for the model developed.

1. A RESONATOR IN AN ACOUSTIC FIELD

Figure 2-1 shows a lumped acoustic model of a single resonator in an acoustic field. The network equations for this system are:

$$p_1 = -Z_1^a U_1 \tag{2-1a}$$

and

$$p_1 = Z_{11}^{ar} U_1 + p_1^b \qquad (2\text{-}1b)$$

where p_1 = acoustic pressure at the surface of the resonator

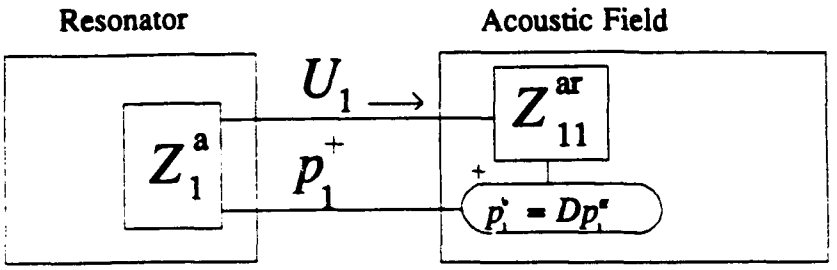

Figure 2-1 Lumped acoustic model of a resonator in an acoustic field.

U_1 = acoustic volume velocity of the resonator

Z_1^a = acoustic impedance of the resonator

Z_{11}^{ar} = acoustic radiation impedance presented to the resonator by the medium with all other active or passive elements blocked

p_1^b = the acoustic pressure acting on the surface of the resonator when it is blocked (i.e. $U_1 = 0$)

D = diffraction constant [Ref. 7]

p_1^{ff} = free-field pressure incident on the resonator, i.e. the pressure that would exist at the location of the resonator if it were not present.

The free-field pressure can be found from

$$p_1^{ff} = \sum_m Z_{1m}^{arf} U_m \tag{2-2}$$

where m increments over all other active and passive elements present and

Z_{1m}^{arf} = the free-field acoustic transfer impedance from element m to the resonator

U_m = acoustic volume velocity of element m.

Bobber [Ref. 7] defines the diffraction constant as the following ratio

$$D_1 = \frac{p_1^b}{p_1^{ff}} \quad . \tag{2-3}$$

The blocked pressure is the average pressure over the surface of the resonator if its volume velocity is zero. The surface pressure is, in general, the sum of the blocked pressure and the radiated pressure, as indicated in Figure 2-1. The radiated pressure is given by

$$p_1^{rad} = U_1 Z_{11}^{ar} \tag{2-4}$$

and so the total pressure at the surface is

$$p_1 = p_1^b + p_1^{rad} = Dp_1^{ff} + U_1 Z_{11}^{ar} \; . \tag{2-5}$$

For notational convenience, we will include the diffraction constant as part

of the acoustic transfer impedance between two elements. Let Z_{nm}^{ar} be the transfer impedance from element m to element n. We can then write

$$p_n^b = \sum_m Z_{nm}^{ar} U_m . \qquad (2\text{-}6)$$

The radiation impedance is a function of the properties of the medium and the physical size and shape of the object radiating into the medium. The input acoustic impedance is a function of the properties of the resonator.

2. A TRANSDUCER IN AN ACOUSTIC FIELD

Figure 2-2 is the lumped acoustic model of a transducer in an acoustic field.

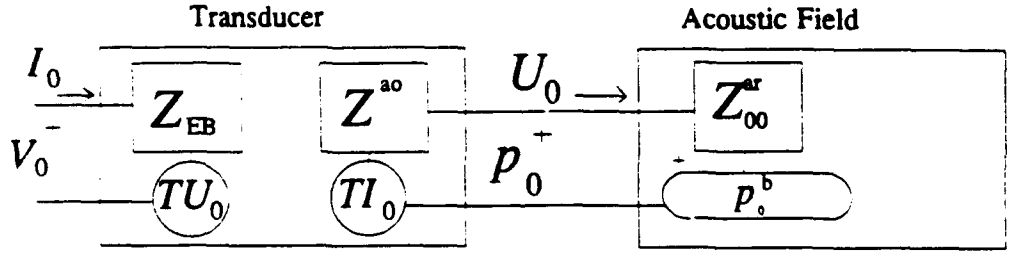

Figure 2-2 Lumped acoustic model of a transducer in an acoustic field.

The network equations for this system are

$$p_0 = T I_0 - Z^{ao} U_0 \qquad (2\text{-}7a)$$

$$p_0 = Z_{00}^{ar} U_0 + p_0^b \qquad (2\text{-}7b)$$

and

$$V_0 = Z_{EB} I_0 - T U_0 \qquad (2\text{-}7c)$$

where p_0 = acoustic pressure at the surface of the transducer

U_0 = acoustic volume velocity of the transducer

Z^{ao} = open-circuit acoustic impedance of the transducer

T = transduction coefficient of the transducer

Z_{00}^{ar} = acoustic radiation impedance presented to the resonator by the medium with all other active or passive elements blocked

p_0^b = the blocked acoustic pressure at the surface of the transducer

Z_{EB} = blocked electrical impedance of transducer

V_0 = voltage across the electrical terminals of the transducer

I_0 = current through the electrical terminals of the transducer.

The blocked acoustic pressure is found as before. The electrical quantities and physical characteristics of the transducer will not be considered further here but are included for completeness. The transducer is taken to be compact and we are interested in the radiation impedance presented to it. The volume velocity of the transducer will be held constant (assumed to be displacement-limited). For a displacement-limited transducer, the power radiated can only be increased by increasing the radiation loading.

3. A TRANSDUCER IN THE PRESENCE OF PASSIVE ELEMENTS

Figure 2-3 is the network model of N interacting passive acoustic resonators coupled to a single transducer by an acoustic field. This model combines the results of

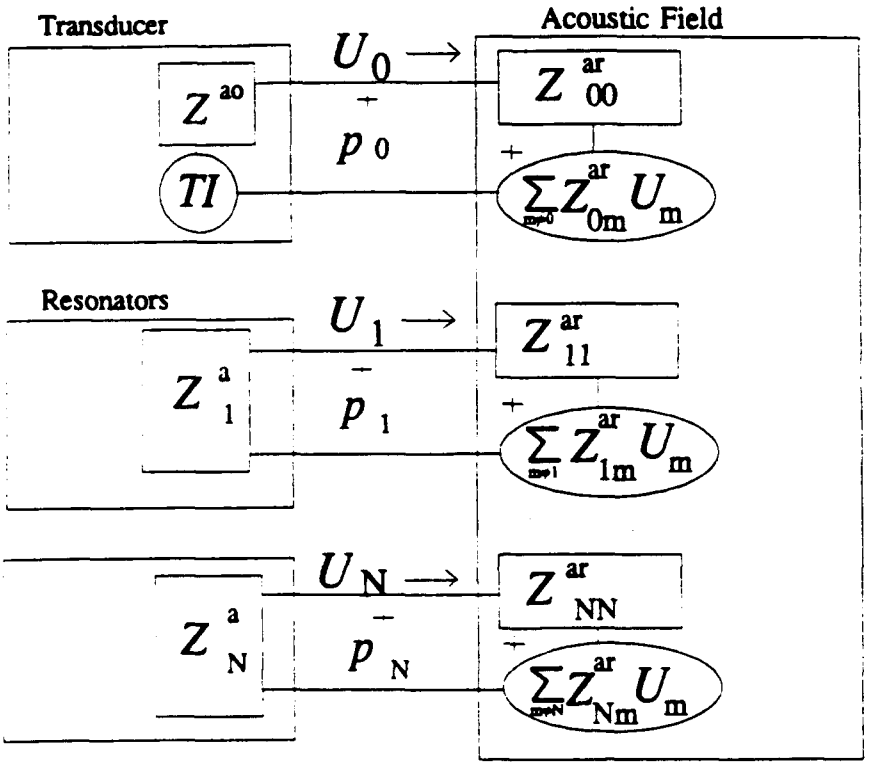

Figure 2-3 Network model of N interacting passive acoustic resonators and a transducer

the previous two sections and allows for interactions between each element and every other element. The network equations are

$$p_0 = T I - Z^{ao} U_0 \qquad (2\text{-}8a)$$

and

$$p_n = -Z_n^a U_n \qquad n=0,1,2,\ldots,N \tag{2-8b}$$

$$p_n = \sum_m Z_{nm}^{ar} U_m \qquad n=1,2,3,\ldots,N \tag{2-8c}$$

where N = number of passive acoustic resonators

p_n = acoustic pressure at the surface of element n

U_n = volume velocity of element n

Z_{nn}^{ar} = acoustic radiation impedance seen by element n with all other active or passive elements blocked

Z_{nm}^{ar} = acoustic transfer impedance from element m to element n.

We are interested in the total acoustic radiation impedance seen by the transducer in the presence of the passive acoustic resonators. This quantity can be defined as follows

$$Z_{total}^{ar} = \frac{p_0}{U_0} . \tag{2-9}$$

Equation 2-8 can be written for the case of N=6 resonators as the following matrix equation

$$\begin{bmatrix} p_0 \\ p_1 \\ p_2 \\ p_3 \\ p_4 \\ p_5 \\ p_6 \end{bmatrix} = \begin{bmatrix} Z_{00}^{ar} & Z_{01}^{ar} & Z_{02}^{ar} & Z_{03}^{ar} & Z_{04}^{ar} & Z_{05}^{ar} & Z_{06}^{ar} \\ Z_{10}^{ar} & Z_{11}^{ar} & Z_{12}^{ar} & Z_{13}^{ar} & Z_{14}^{ar} & Z_{15}^{ar} & Z_{16}^{ar} \\ Z_{20}^{ar} & Z_{21}^{ar} & Z_{22}^{ar} & Z_{23}^{ar} & Z_{24}^{ar} & Z_{25}^{ar} & Z_{26}^{ar} \\ Z_{30}^{ar} & Z_{31}^{ar} & Z_{32}^{ar} & Z_{33}^{ar} & Z_{34}^{ar} & Z_{35}^{ar} & Z_{36}^{ar} \\ Z_{40}^{ar} & Z_{41}^{ar} & Z_{42}^{ar} & Z_{43}^{ar} & Z_{44}^{ar} & Z_{45}^{ar} & Z_{46}^{ar} \\ Z_{50}^{ar} & Z_{51}^{ar} & Z_{52}^{ar} & Z_{53}^{ar} & Z_{54}^{ar} & Z_{55}^{ar} & Z_{56}^{ar} \\ Z_{60}^{ar} & Z_{61}^{ar} & Z_{62}^{ar} & Z_{63}^{ar} & Z_{64}^{ar} & Z_{65}^{ar} & Z_{66}^{ar} \end{bmatrix} \begin{bmatrix} U_0 \\ U_1 \\ U_2 \\ U_3 \\ U_4 \\ U_5 \\ U_6 \end{bmatrix} . \qquad (2\text{-}10)$$

In order to simplify the notation, we will write equation 2-10 as

$$\begin{bmatrix} p_0 \\ \{p_n\} \end{bmatrix} = \begin{bmatrix} Z_{00}^{ar} & \{Z_{m0}^{ar}\}^T \\ \{Z_{n0}^{ar}\} & [Z_{nm}^{ar}] \end{bmatrix} \begin{bmatrix} U_0 \\ \{U_m\} \end{bmatrix} \qquad (2\text{-}11)$$

where $\{X\}$ is a 1xN column matrix

$[X]$ is a NxN square matrix

and the superscript "T" indicates the transpose of a matrix.

In order to find Z_{total}^{ar} ,first we replace $\{p_n\}$ by $\{-Z_n^a U_n\}$ and normalize by U_0,

resulting in the following equation:

$$\begin{bmatrix} Z_{total}^{ar} \\ \{0\} \end{bmatrix} = \begin{bmatrix} Z_{00}^{ar} & \{Z_{m0}^{ar}\}^T \\ \{Z_{n0}^{ar}\} & [Z_{nm}^{ar} + Z_n^a \delta_{nm}] \end{bmatrix} \begin{bmatrix} 1 \\ U_m^{rel} \end{bmatrix} , \qquad (2\text{-}12)$$

where $\delta_{nm} = \begin{cases} 1 & n = m \\ 0 & n \neq m \end{cases}$

and $U_m^{rel} = \frac{U_m}{U_0}$.

We can represent the matrix of equation 2-12 as the following system of equations:

$$Z_{total}^{ar} = Z_{00}^{ar} + \left\{Z_{m0}^{ar}\right\}^T \left\{U_m^{rel}\right\} \tag{2-13}$$

and

$$\{0\} = \left\{Z_{n0}^{ar}\right\} + \left[Z_{nm}^{ar} + Z_n^a \delta_{nm}\right] \left\{U_m^{rel}\right\} \qquad n,m=1,2,\ldots,N . \tag{2-14}$$

Solving for $\left\{U_m^{rel}\right\}$ in equation 2-14 yields

$$\left\{U_m^{rel}\right\} = -\left[Z_{nm}^{ar} + Z_n^a \delta_{nm}\right]^{-1} \left\{Z_{n0}^{ar}\right\} . \tag{2-15}$$

Equation 2-15 gives the relative volume velocities of each resonator with respect to the transducers volume velocity. We substitute equation 2-15 into equation 2-13 to obtain the following expression for Z_{total}^{ar}:

$$Z_{total}^{ar} = Z_{00}^{ar} - \left\{Z_{m0}^{ar}\right\}^T \left[Z_{nm}^{ar} + Z_n^a \delta_{nm}\right]^{-1} \left\{Z_{n0}^{ar}\right\} . \tag{2-16}$$

The total radiation impedance presented to the transducer will be used to find the gain in radiation resistance with resonators present.

4. THE INPUT PARAMETERS

The physical parameters that we must provide in the model developed above are (1) the acoustic impedance of each resonator, (2) the transfer impedance of each element in the presence of other elements and with the other elements blocked, (3) the physical characteristics of the medium (hydrostatic pressure, sound speed, etc.). The required equations are developed later in this chapter. The equations for the measures of effectiveness chosen to evaluate the resonator systems are developed in the sections that follow.

B. GAIN IN RADIATION RESISTANCE

The total power radiated into the water by a simple source is [Ref. 8]

$$\prod = \frac{1}{T_0} \int_0^{T_0} Re[f]\ Re[u_0]dt \qquad (2\text{-}17)$$

where f = force of the fluid on the source

u_0 = particle velocity at the surface of the source

T_0 = period of harmonic motion.

In terms of the variables used in this paper, the total power delivered to the acoustic field by a transducer in the presence of N passive resonators is given by

$$\prod_N = \frac{1}{2} U_0^2\ Re[Z_{total}^{ar}] \ . \qquad (2\text{-}18)$$

The gain in power delivered to the acoustic field due to the presence of the resonators can be defined as [Ref. 4]

$$Gain = \frac{total\ power\ delivered\ with\ the\ resonators\ present}{total\ power\ delivered\ without\ the\ resonators} . \quad (2\text{-}19)$$

For a compact source, the radiated acoustic power in the absence of the resonators can be approximated by

$$\Pi_0 = \frac{1}{2} U_0^2 \, Re[Z_{00}^{ar}] . \quad (2\text{-}20)$$

Then we can write equation 2-19 as

$$Gain = \frac{Re[Z_{total}^{ar}]}{Re[Z_{00}^{ar}]} . \quad (2\text{-}21)$$

We will refer to this quantity as the gain in radiation resistance, or simply gain. The gain in radiation resistance is an important measure of effectiveness because it quantifies the additional radiated power due to the presence of passive acoustic radiators. We will use this quantity to evaluate the benefit of using passive acoustic radiators in various configurations.

C. BEAM PATTERNS AND DIRECTIVITY

The directivity of a transducer due to the presence of passive acoustic resonators can be determined by analyzing the far-field beam pattern. To find the beam pattern we find the radiated pressure due to each element at far-field points in various directions. For a compact source, we can calculate the field pressure due to a single element as

$$p_n^{field} = U_n Z_{nn}^{ar} \frac{a_n}{r_n} \frac{e^{-jkr_n}}{e^{-jka_n}} \tag{2-22}$$

where p_n^{field} = acoustic pressure at a field point due to element n

a_n = radius of element n

r_n = distance to the field point from the acoustic center of element n.

The total pressure at the field point due to the transducer and system of resonators is then

$$p_{tot}^{field}(r,\theta,\phi) = \sum_{n=0}^{N} p_n^{field}(r,\theta,\phi) \tag{2-23}$$

where $p_n^{field}(r,\theta,\phi)$ = the pressure at the field point specified by the spherical coordinates (r,θ,ϕ) due to element n.

In the plots which will be presented, the above far-field pressure is normalized by the pressure at the same point due to the transducer alone. What is plotted, then is the following function, termed BP(θ,ϕ):

$$BP(\theta,\phi) = \lim_{kr \gg 1} \frac{\left| p_{tot}^{field}(r,\theta,\phi) \right|}{\left| p_0^{field}(r,\theta,\phi) \right|} . \tag{2-24}$$

We will plot the beam pattern defined by equation 2-24 in three dimensions in order to easily see what is the effect of the resonators on the pressure field. We will also plot the beam pattern on a log scale in the form of a polar plot. Polar plots are the traditional

method of presenting a beam pattern. In this case 0 dB will represent the sound pressure level of the transducer with no resonators present.

A measure of how well the system projects power along an acoustic axis is the directivity index. The directivity index is defined as [Ref. 8]

$$DI = 10 \log_{10}\left[\frac{p_{ax}^2(r)}{p_s^2(r)}\right] \tag{2-25}$$

where $p_{ax}(r)$ = acoustic pressure due to the directional source at a range r along the acoustic axis

$p_s(r)$ = acoustic pressure, at a range r, due to a spherical source radiating the same acoustic power as the directional source.

In terms of our equations, the directivity index can be show to be

$$DI = 20 \log_{10}\left(BP(\theta_{ax},\phi_{ax})\right) - 20\log_{10}\left(\sqrt{Gain}\right) \tag{2-26}$$

where θ_{ax} and ϕ_{ax} indicate the spherical angles along the acoustic axis.

D. GAS-FILLED BUBBLES AS PASSIVE ACOUSTIC RADIATORS

Tolstoy and Ellsworth both considered air-filled bubbles as passive acoustic resonators in their papers. Here, we will consider air-filled bubbles at a hydrostatic pressure $P_0 = 1$ atm (just below the surface). We will assume a sound speed in water

of $c = 1500$ meters per second and a density in water of $\rho_0 = 998$ kg/m^3. The ratio of specific heats for air is $\gamma = 1.4$.

In addition to the above constants, we require the acoustic impedance of each resonator and the transfer impedances between all elements. The required impedances for air-filled bubbles are developed below.

The mechanical stiffness of an air bubble in water is [Ref. 8]

$$s = 12 \pi a \gamma P_0 \tag{2-27}$$

where a is the radius of the bubble. This stiffness can be represented as an acoustic impedance as follows

$$Z_n^a = -j\frac{3 \gamma P_0}{S c k a} \tag{2-28}$$

where S = surface area of the bubble

k = wavenumber in water.

We have only included the adiabatic stiffness of the air, since the effects of surface tension, non-adiabatic expansion and contractions, and losses due to viscosity can be neglected for bubbles larger than 1 mm [Ref. 9] and frequencies below 40 kHz [Ref. 8].

The resonant frequency of a bubble in water is [Ref. 8]

$$\omega_0 = \frac{1}{a}\sqrt{\frac{3 \gamma P_0}{\rho_0}} \; . \tag{2-29}$$

We will prefer to consider dimensionless quantities such as the wavenumber times distance. Equation 2-29 can then be expressed as

$$ka_r = \sqrt{\frac{3\,\gamma\,P_0}{\rho_0\,c^2}} \quad . \tag{2-30}$$

For the values specified above, the resonant value of ka is $ka_r = 0.01377$.

The acoustic self-impedance seen by element n is [Ref. 8]

$$Z_{nn}^{ar} = \frac{\rho_0 c}{S} \frac{ka_n}{\sqrt{1 + (ka_n)^2}} e^{j\theta} \tag{2-31}$$

where $\cot(\theta) = ka_n$. This can be easily rewritten as

$$Z_{nn}^{ar} = \frac{\rho_0 c}{S} \frac{jka_n}{1+jka_n} \quad . \tag{2-32}$$

The transfer impedance from element m to element n is

$$Z_{nm}^{ar} = Z_{mm}^{ar} D_n \frac{ka_m}{kl_{nm}} e^{j(ka_m - kl_{nm})} \tag{2-33}$$

where l_{nm} is the distance between the acoustic centers of elements m and n. The diffraction constant for a sphere of radius a_n is [Ref. 7]

$$D_n = \frac{e^{jka_n}}{1+jka_n} \quad . \tag{2-34}$$

We have taken the transducer radius, a_0, to satisfy $ka_0 = 0.2$. This is a typical value for a low frequency transducer. Later we will show that the results are not sensitive to this choice over a large range of values. This value of transducer radius was used for all calculations unless otherwise noted.

E. OTHER PASSIVE ACOUSTIC RADIATORS

The network model developed above is general and can be used for a variety of passive acoustic radiators. Any compact resonator that can be characterized by a stiffness alone, such as an air bubble in water, can use the impedances developed for the bubble with the appropriate choice of ka_r. In addition to the air bubble at 1 atm ambient pressure, we have chosen to perform calculations for a bubble-like resonator with a value of $ka_r = 0.1$ (which corresponds to an air bubble at 50 atm ambient pressure). We can expect that a very thin-shelled object made of steel or aluminum, an air balloon, or air bladder might be built with these characteristics. We have not attempted to devise or construct such a system, but rather present results to determine whether one should be built. We will compare the results for air bubbles at 1 atm ambient pressure and resonators with $ka_r = 0.1$.

III. THE CIRCULAR CONFIGURATIONS

In this chapter, we present the results for the two circular configurations previously analyzed by Ellsworth [Ref. 4]. The tables of results presented below were created using more accurate numerical techniques than those used by Ellsworth. Also, the equations used require fewer assumptions. Specifically, (1) we use an exact equation for the radiation impedance from a sphere (rather than an approximate formula), (2) we take into account the diffraction constant relating the blocked pressure to the incident pressure wave, (3) we used a gradient search method to find the maximum gain as a function of the free parameters rather than reporting the maximum found over the coarse grid of parameter values, (4) we calculate the directivity index for each case considered, and (5) we plot three-dimensional beam patterns in order to better visualize the effect of passive acoustic resonators on the acoustic field. Ellsworth provided plots of gain in radiation resistance and beam patterns for the case N=4. In this thesis we present graphs for the case N=6. It will be shown that the six resonator case is superior to the four resonator case, and is in fact the best choice. In the following sections we present results for the planar and the conical configurations.

A. THE PLANAR CONFIGURATION

1. THE GEOMETRY

Figure 3-1 shows the geometry of the planar circular configuration for the case of six passive acoustic resonators. The radius of the circle is R and the transducer is in the plane of the resonators (x-y plane). We are interested in dimensionless distances, so the radius of the circle will be referred to in terms of wavenumber times the radius, kR. The dimensionless radius of each resonator is ka and the dimensionless radius of the transducer is ka_0 . We assume a value for the transducer radius of

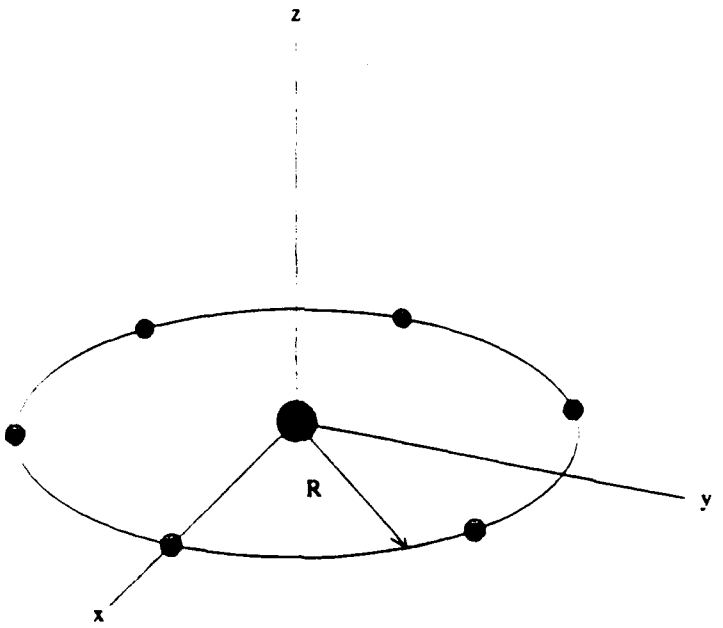

Figure 3-1 Geometry for the planar configuration with six resonators. The plot is drawn to scale for resonators with $ka \approx 0.1$.

ka_0=0.2. Later we will demonstrate that the results are independent of the value chosen over the range of interest.

2. GAIN IN RADIATION RESISTANCE

Figure 3-2 shows a three-dimensional surface plot and contour plot of the gain in radiation resistance versus *ka* and *kR* for six air bubbles, at 1 atm ambient pressure, in the configuration of Figure 3-1. The gain has a peak value of 1.95 at *ka* = 0.0138 and *kR* = 2.87. The increasing value of gain as *kR* gets small is not interesting because of the expected divergent behavior [Ref. 4]. Inspection of the gain plot reveals that the peak in gain is very narrow in the *ka*-direction. The reason is the very sharp peak in the tuning curve for a resonant bubble. The Q of a resonant bubble is about $1/ka_r$ [Ref. 8].

The gain in radiation resistance was also plotted for a bubble-like passive acoustic resonator whose resonant value of *ka* is 0.1. This is shown in Figure 3-3. An air bubble at 50 atm hydrostatic pressure will have ka_r=0.1. It is also expected that a more depth-independent resonator such as a thin-shell could be constructed with ka_r=0.1. The Q for this case is about 10 (as compared to about 70 for an air bubble at 1 atm ambient pressure.) Figure 3-3 shows a much broader range of *ka* values with substantial ($\geq$1.5) gain. The implication of these observations is that using air bubbles at 1 atm ambient pressure would not be practical, but that using resonators with ka_r=0.1 could result in a practical application.

Table 3-1 shows numerical results for the planar configuration for two through ten resonators at 1 atm ambient pressure. The calculations were performed using

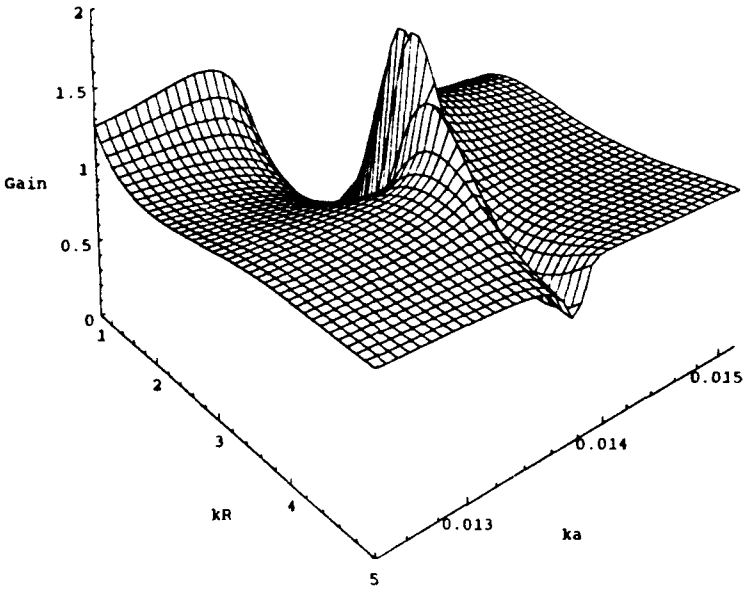

(a)

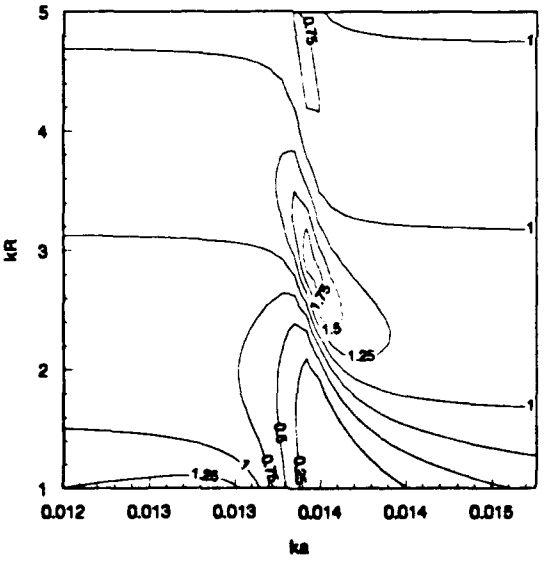

(b)

Figure 3-2 Gain in radiation resistance versus *ka* and *kR* for the planar configuration with six air bubbles at 1 atm ambient pressure (a) 3D surface plot (b) contour plot

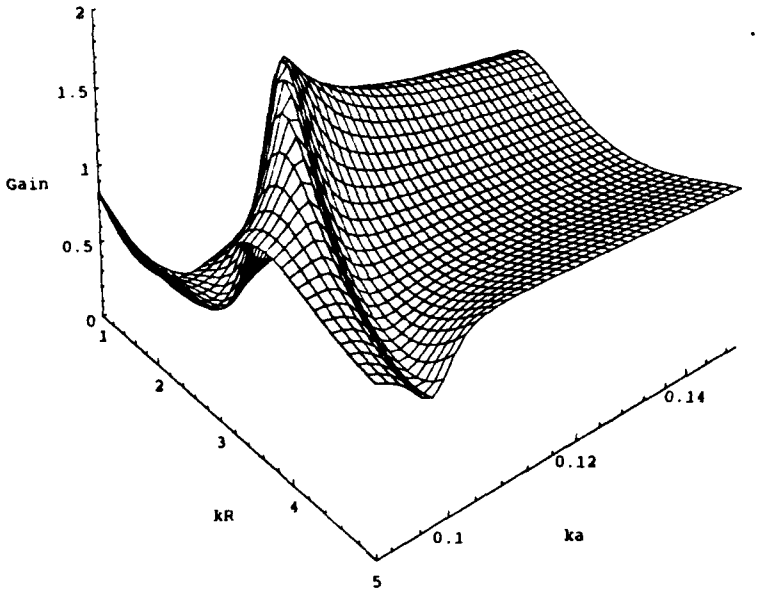

(a)

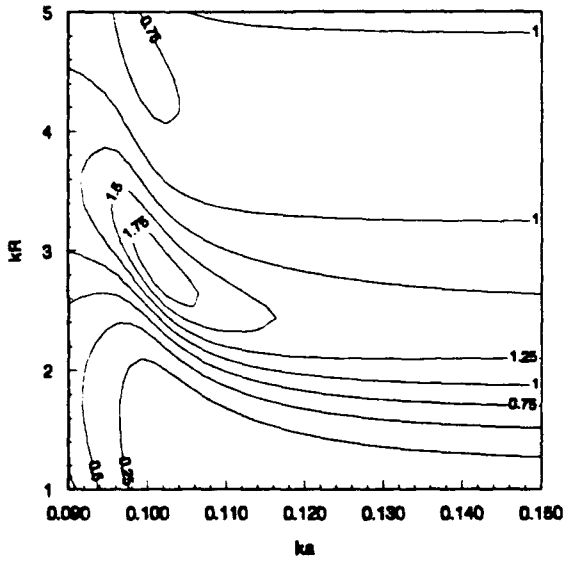

(b)

Figure 3-3 Gain in radiation resistance versus *ka* and *kR* for the planar configuration for six resonators with $ka_r = 0.1$ (a) 3D surface plot (b) contour plot

N	ka	kR	$Gain$	$\mid U^{rel} \mid$	$N \mid U^{rel} \mid$	$\angle U^{rel}$	DI
2	0.0138092	2.65	1.26	0.386	0.773	90.0	1.2
3	0.0138041	2.69	1.59	0.573	1.72	90.0	4.2
4	0.0138111	2.82	1.87	0.636	2.55	90.0	6.2
5	0.0138244	2.86	1.95	0.553	2.76	90.0	6.7
6	0.0138355	2.87	1.95	0.465	2.79	90.0	6.7
7	0.0138427	2.87	1.95	0.398	2.79	90.0	6.7
8	0.0138471	2.87	1.95	0.349	2.79	90.0	6.7
9	0.0138494	2.87	1.95	0.310	2.79	90.0	6.7
10	0.0138499	2.87	1.95	0.279	2.79	90.0	6.7

Table 3-1 Planar configuration results for air bubbles at 1 atm ambient pressure.

ka_0	ka	kR	$Gain$	$\mid U^{rel} \mid$	$\angle U^{rel}$
0.01	0.0138355	2.86783	1.95490	0.474090	90.0
0.025	0.0138355	2.86783	1.95490	0.473965	90.0
0.05	0.0138355	2.86785	1.95488	0.473517	90.0
0.075	0.0138355	2.86790	1.95482	0.472770	90.0
0.1	0.0138355	2.86801	1.95472	0.471723	90.0
0.2	0.0138355	2.86927	1.95350	0.464611	90.0
0.5	0.0138342	2.88818	1.93501	0.420116	90.0
0.75	0.0138342	2.92865	1.89464	0.367996	90.0

Table 3-2 Planar configuration results for six resonators allowing ka_0 to vary.

Mathematica with a precision of about ten significant digits (the working precision was twenty significant digits). Fewer digits are shown in the table because they are not of general interest. Note that the table indicates that there is no additional increase in gain beyond six resonators. This is in part the basis for our claim that, for the circular configurations, six resonators is the best choice. Table 3-1 also reveals that when the gain reaches its maximum value, the total volume velocity of the resonators ($N \cdot |U^{el}|$) remains constant with increasing numbers of resonator. The phase of the volume velocity of each resonator ($\angle U^{el}$) is 90° relative to the transducer. We will make use of this fact in the conical configuration.

Recall that the calculations for Figures 3-1 and 3-2 and Table 3-1 are for ka_0=0.2. Table 3-2 shows the results for six resonators where we allow ka_0 to vary.

N	ka	kR	*Gain*	$\lvert U^{el} \rvert$	$N \lvert U^{el} \rvert$	$\angle U^{el}$	*DI*
2	0.0996243	2.65	1.26	0.388	0.776	90.0	1.2
3	0.0993435	2.70	1.59	0.576	1.73	90.0	4.2
4	0.0997272	2.82	1.87	0.639	2.56	90.0	6.2
5	0.100477	2.86	1.94	0.556	2.78	90.0	6.7
6	0.101117	2.87	1.95	0.467	2.80	90.0	6.7
7	0.101548	2.87	1.95	0.400	2.80	90.0	6.7
8	0.101813	2,87	1.95	0.350	2.80	90.0	6.7
9	0.101949	2.87	1.95	0.311	2.80	90.0	6.7
10	0.101981	2.87	1.95	0.280	2.80	90.0	6.7

Table 3-3 Planar configuration results for resonators with ka_r=0.1.

The results show that, over a large range of values, the gain in radiation resistance is independent of the value of ka_0 chosen. The numerical results for resonators with ka_r=0.1 are shown in Table 3-3. The values of kR, Gain, U^{rel}, and directivity index (DI) remain the same as in Table 3-1. The values of ka are different but it can be shown that the ratio ka/ka_r is the same. This indicates that over a large range of values, the gain in radiation resistance is independent of the value of ka_r for bubble-like resonators.

3. BEAM PATTERNS AND DIRECTIVITY

The three-dimensional beam pattern can be found by plotting equation 2-24 over all spherical angles. Figure 3-4 is the three-dimensional far-field beam pattern for

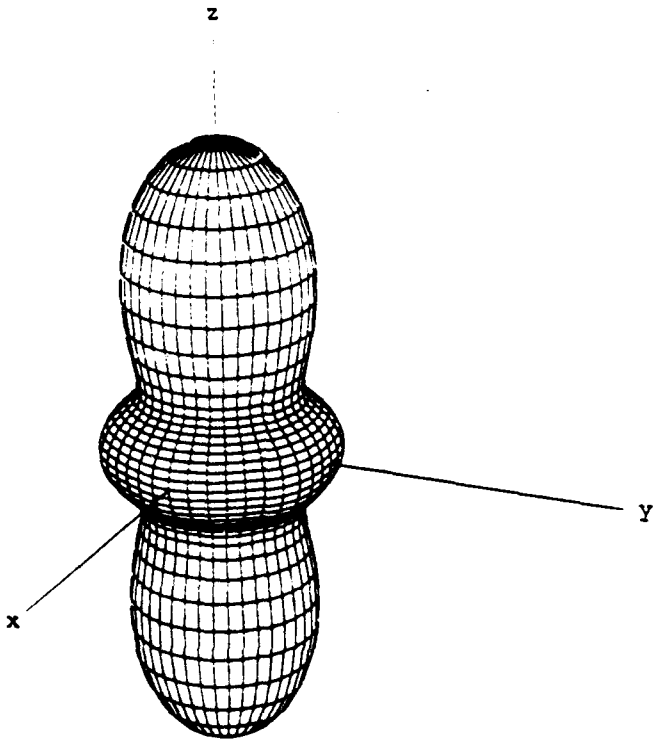

Figure 3-4 Three-dimensional beam pattern for planar configuration with six resonators at 1 atm ambient pressure.

the planar configuration with six air bubbles at 1 atm ambient pressure. The three-dimensional (3D) beam pattern provides the reader with an idea of what the pressure field will look like in 3D space without having to resort to multiple 2D plots in various planes. Now that we know what the beam pattern looks like we can better utilize our polar plots to analyze the results. From the 3D plot alone, we can see that there is some significant directivity along the acoustic axis (in this case the positive z-axis). We can also see that the pressure field is symmetric about the z-axis and the x-y plane.

The usual method of presenting a beam pattern is the dB polar plot. Figure 3-5 is a polar plot of the beam pattern for the planar configuration with six resonators.

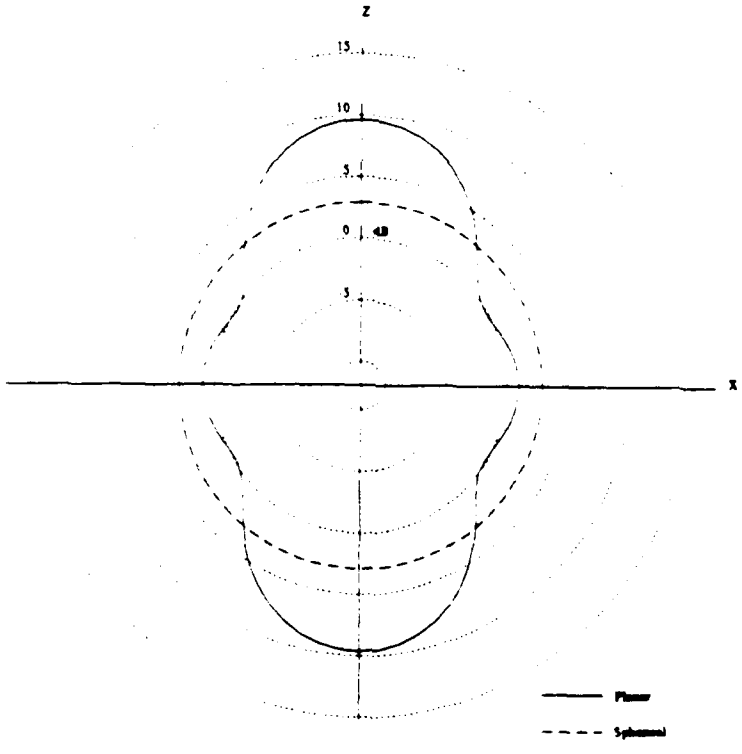

Figure 3-5 Polar plot of the beam pattern for the planar configuration with six resonators at 1 atm ambient pressure.

The zero dB reference is the pressure that would exist due to the transducer if no passive elements were present. The dashed line represents the sound pressure level that would exist due to a spherical source radiating the same acoustic power as the transducer does in the presence of the passive elements. The directivity index, defined by equation 2-26, can be read directly from Figure 3-5 as the difference in dB between the sound pressure level of the transducer in the presence of passive acoustic radiators and that of the spherical source radiating the same acoustic power. The directivity index in this case is 6.7 dB. Tables 3-1 and 3-3 list the directivity index for the planar configuration for two through ten resonators at 1 atm ambient pressure and for ka_r=0.1.

B. THE CONICAL CONFIGURATION

1. THE GEOMETRY

The relative volume velocity of the passive acoustic resonators was noted in the last section to be ninety degrees out of phase with the transducer volume velocity. We also noted that the far-field beam pattern was symmetric about the x-y plane. For a directional source, we usually want the sound energy to be directed along a single acoustic axis with any side or back lobes minimized. We make use of the phase of the resonators' relative volume velocity in the conical configuration to improve the directivity of the system. In the conical configuration the transducer is displaced one-quarter wavelength out of the plane of the resonators. Figure 3-6 shows the geometry of the conical configuration for the case of six passive acoustic resonators. The dimensionless

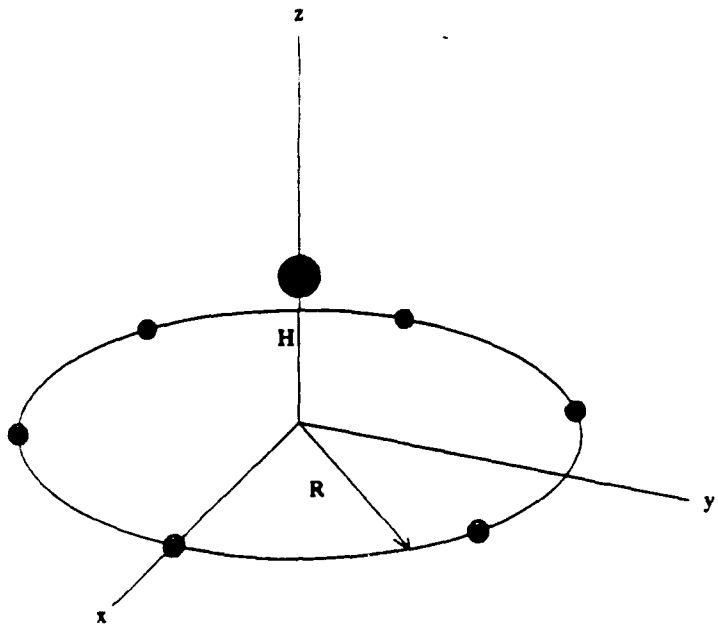

Figure 3-6 Geometry of the conical configuration with six resonators.

radius of the circle of resonators is kR and the dimensionless height of the transducer is $kH = \pi/2$.

2. GAIN IN RADIATION RESISTANCE

Surface and contour plots of the gain in radiation resistance for the conical configuration with six resonators at 1 atm ambient pressure are shown in Figure 3-7. The plots are similar to the planar configuration plots except that the gain is not as large. The peak in gain seen in Figure 3-7 is 1.82 at ka=0.0138 and kR=2.69. The value of ka is 1.005 times the resonant value for a single bubble at 1 atm ambient pressure and is approximately the same as the value of ka for maximum gain in the planar configuration. As in the planar configuration, the peak in gain is very narrow in the

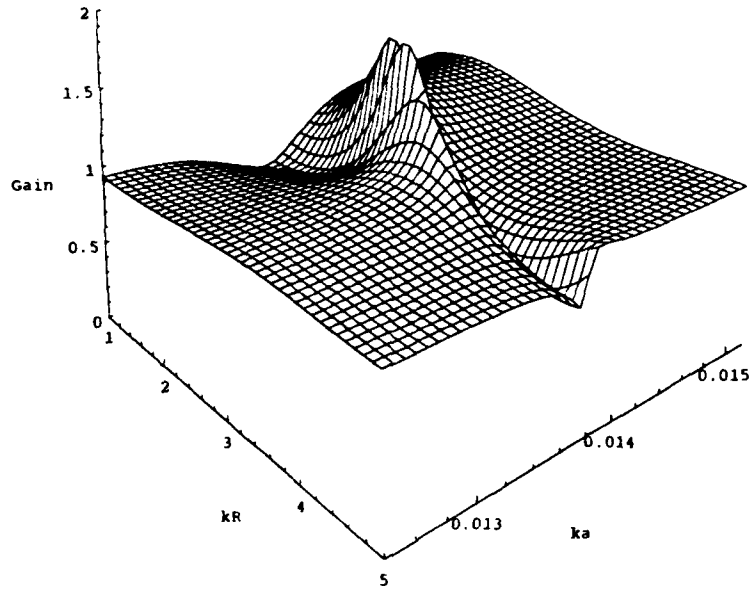

(a)

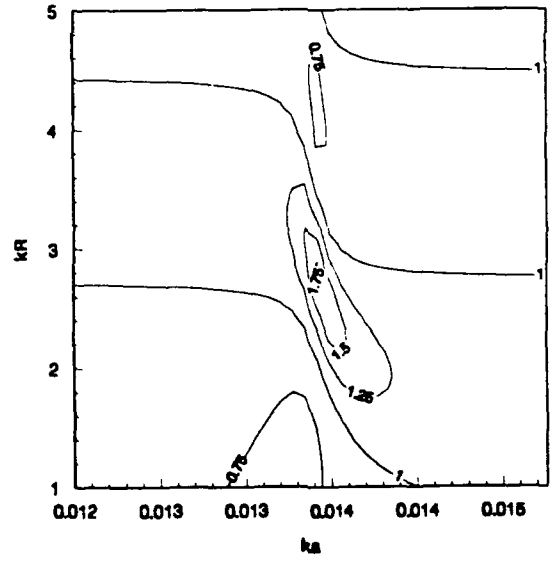

(b)

Figure 3-7 Gain in radiation resistance versus *ka* and *kR* for the conical configuration with six resonators at 1 atm ambient pressure (a) 3D surface plot, (b) contour plot

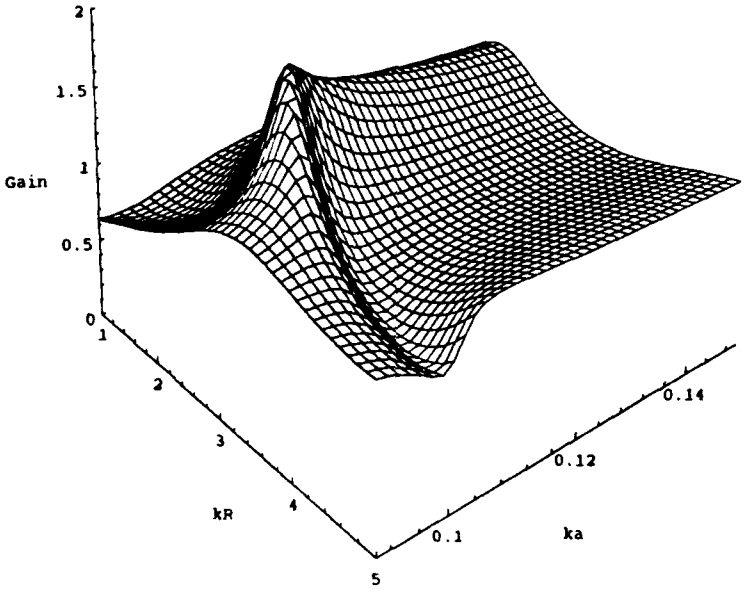

(a)

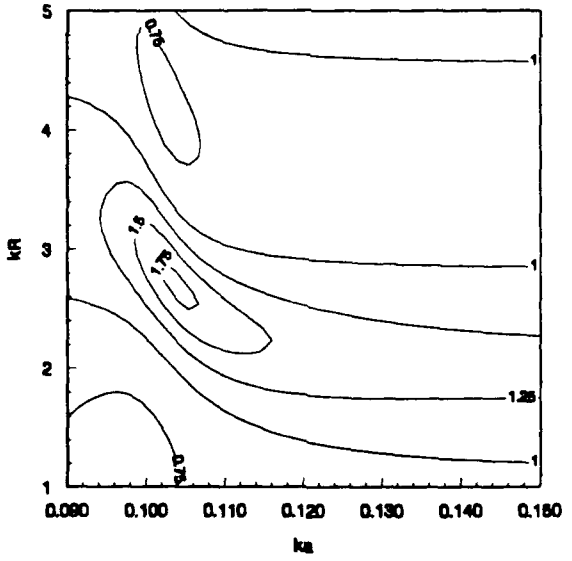

(b)

Figure 3-8 Gain in radiation resistance versus *ka* and *kR* for the conical configuration with six resonators for $ka_r = 0.1$ (a) 3D surface plot (b) contour plot

ka-direction. Figure 3-8 shows the surface and contour plots for the conical configuration where the resonators are assumed to have a value of ka_r=0.1. Once again, the peak has broader support in the *ka*-direction for ka_r=0.1.

The numerical results for the conical configuration are given in Tables 3-4, 3-5, and 3-6. Table 3-4 gives the results for air bubbles at 1 atm ambient pressure for

N	*ka*	*kR*	*Gain*	$\lvert U^{rel} \rvert$	$N \lvert U^{rel} \rvert$	$\angle U^{rel}$	*DI*
2	0.0138079	2.29	1.29	0.421	0.841	90.0	4.3
3	0.0138038	2.49	1.58	0.570	1.71	90.0	6.7
4	0.0138115	2.65	1.78	0.589	2.36	90.0	8.1
5	0.0138238	2.69	1.82	0.501	2.51	90.0	8.4
6	0.0138330	2.69	1.82	0.420	2.52	90.0	8.4
7	0.0138384	2.69	1.82	0.360	2.52	90.0	8.4
8	0.0138409	2.69	1.82	0.315	2.52	90.0	8.4
9	0.0138413	2.69	1.82	0.280	2.52	90.0	8.4
10	0.0138399	2.69	1.82	0.252	2.52	90.0	8.4

Table 3-4 Conical configuration results for air bubbles at 1 atm ambient pressure.

two through ten resonators. The conical configuration, like the planar configuration, does not provide any additional gain in radiation resistance for more than six resonators. Table 3-5 gives the results for six resonators in a conical configuration where we allow ka_0 to vary from the usual value of 0.2. The gain in radiation resistance does not vary significantly with the value of ka_0 chosen. Table 3-6 presents the results for the conical

ka_0	ka	kR	$Gain$	$\lvert U^{rel} \rvert$	$\angle U^{rel}$
0.01	0.013833	2.69149	1.82404	0.428152	90.0
0.025	0.013833	2.69149	1.82402	0.428040	90.0
0.05	0.013833	2.69151	1.82404	0.427641	90.0
0.075	0.013833	2.69155	1.82403	0.426980	90.0
0.1	0.013833	2.69165	1.82402	0.426062	90.0
0.2	0.013833	2.69275	1.82393	0.419965	90.0
0.5	0.013833	2.70910	1.82189	0.38413	90.0
0.75	0.013833	2.74319	1.81422	0.344514	90.0

Table 3-5 Conical configuration results for six resonators allowing ka_0 to vary.

N	ka	kR	$Gain$	$\lvert U^{rel} \rvert$	$N \lvert U^{rel} \rvert$	$\angle U^{rel}$	DI
2	0.0995492	2.29	1.29	0.423	0.845	90.0	4.2
3	0.0993290	2.49	1.58	0.573	1.72	90.0	6.7
4	0.0997511	2.65	1.79	0.592	2.37	90.0	8.1
5	0.100443	2.69	1.82	0.504	2.52	90.0	8.4
6	0.100973	2.69	1.82	0.422	2.53	90.0	8.4
7	0.101288	2.69	1.82	0.362	2.53	90.0	8.4
8	0.101438	2.69	1.82	0.317	2.53	90.0	8.4
9	0.101459	2.69	1.82	0.281	2.53	90.0	8.4
10	0.101376	2.69	1.82	0.253	2.53	90.0	8.4

Table 3-6 Conical configuration results for passive acoustic resonators with ka_r=0.1.

configuration with resonators having a value of ka_r=0.1. The values of kR, Gain, U^{rel}, and DI remain about the same as in Table 3-4. While the values of ka differ, the ratio ka/ka_r is the same for both the 1 atm bubble and the ka_r=0.1 resonator.

Note that, for four or more resonators, the planar configuration has a larger gain in radiation resistance than the conical configuration with the same number of resonators. Calculations show that for four or more resonators, the maximum gain always occurs when the transducer is in the plane of the resonators.

3. BEAM PATTERNS AND DIRECTIVITY

Figure 3-9 shows the three-dimensional far-field beam pattern, defined by equation 2-24 and plotted over all spherical angles. The improvement over the planar configuration is obvious. We traded a small fraction of the gain in radiation resistance for a large increase in directivity. In addition to concentrating sound energy along an acoustic axis, the conical configuration also has smaller side and back lobes than the planar configuration. Figure 3-10 is the polar dB plot of the conical configuration with six resonators at 1 atm ambient pressure. From Figure 3-10 we note that the conical configuration concentrates 3 dB more sound pressure along the acoustic axis than the planar configuration. This represents a doubling of the acoustic intensity.

The directivity index is determined from Figure 3-10 as a described in the last section. The directivity index for six resonators is 8.4 dB. Tables 3-4 and 3-6 list the directivity index for two through ten resonators at 1 atm ambient pressure and for ka_r=0.1. The directivity index, like the gain, does not increase with more resonators past its value for six resonators. The high gain in radiation resistance and high

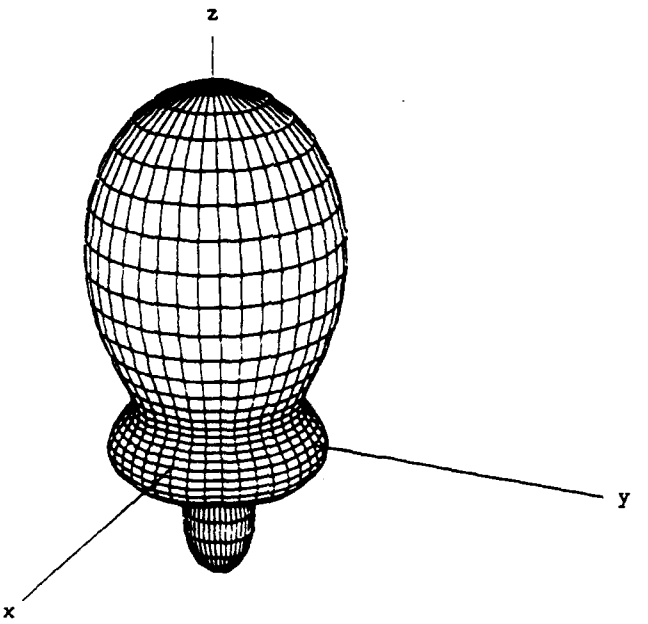

Figure 3-9 Three-dimensional beam pattern for the conical configuration with six resonators at 1 atm ambient pressure.

directivity index make the conical configuration the best choice for a system design. As we will see in the following chapters, the 3D beam pattern for the conical configuration is the most desirable of the configurations considered.

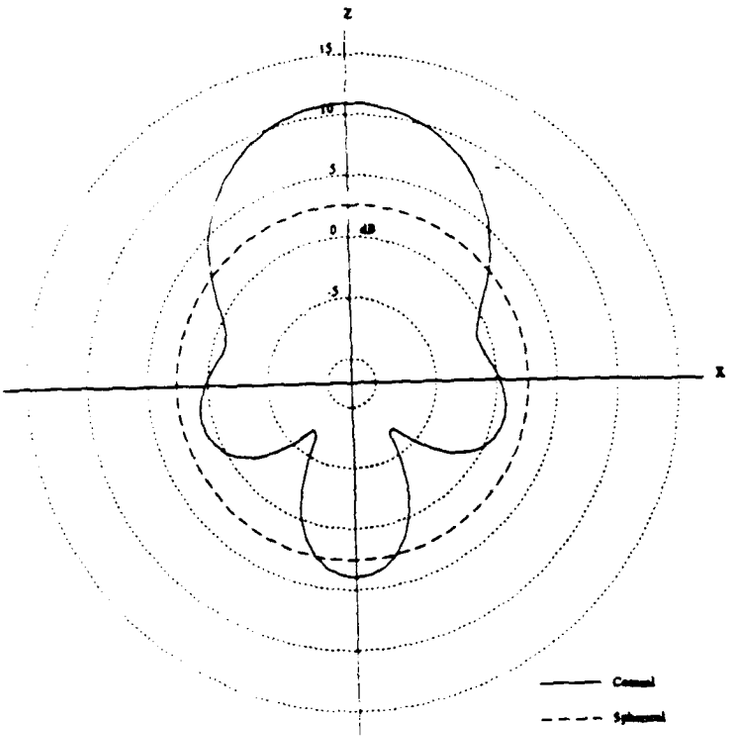

Figure 3-10 Polar plot of the beam pattern on a dB scale for the conical configuration with six resonators at 1 atm ambient pressure.

IV. LINE CONFIGURATION TYPE I

In this chapter and the next two, we extend the work done by Ellsworth by considering linear configurations of passive acoustic resonators. The motivation is to investigate whether a linear configuration offers any improvement in power radiated and directivity compared to a circular configuration. We present results for six resonators for easy comparison to the results in the last chapter. The first line configuration considered, termed line configuration type I, consists of a line of equally spaced resonators on only one side of the transducer. In the next chapter, we consider an equal number of resonators on either side of a transducer in a line (line type II). In Chapter VI, we will consider a Yagi-Uda [Ref. 5] array of resonators (line type III).

A. THE GEOMETRY

Figure 4-1 shows the line configuration type I with six resonators. The transducer is at the origin of the coordinate system and the resonators are along the positive x-axis. The dimensionless distance from the transducer to the first resonator is kL. The dimensionless distance between resonators is kl. The transducer radius is $ka_0=0.2$. Each passive acoustic resonator has radius ka_n, where the subscript n indicates the individual resonator.

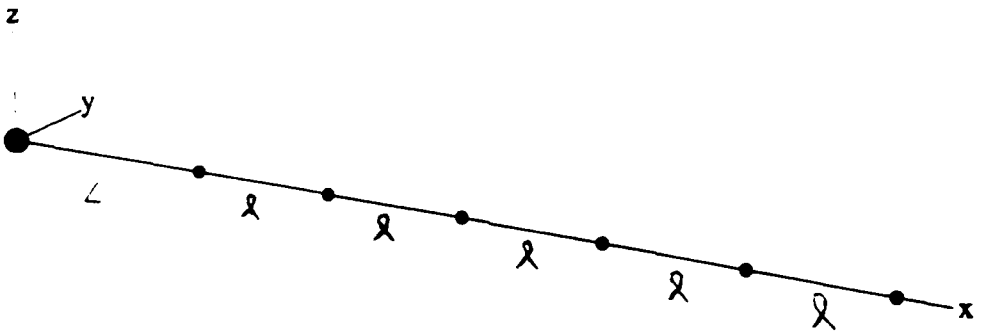

Figure 4-1 Geometry of the line configuration type I with six resonators.

B. GAIN IN RADIATION RESISTANCE

Figure 4-2 shows the gain in radiation resistance presented to the transducer in the presence of a system of six passive acoustic radiators arranged in line configuration type I. The gain in radiation resistance is plotted versus kL and kl with ka held constant at the value that provides maximum gain for a finite value of kL. The maximum considered is the one at $kL=3.6$ and $kl=2.5$, for which $ka=0.01373$. The gain at this point is 1.22 (compared to the conical configuration with a gain of 1.82 for six resonators). The peaks that occur in the gain as kL goes to zero were only briefly considered. This is discussed in the next section. A plot of the gain in radiation resistance versus kL and kl for $ka=ka_r=0.1$ is indistinguishable from Figure 4-2 and is not presented here. We expect that, as for the circular configurations, the $ka_r=0.1$ case is preferable because the range

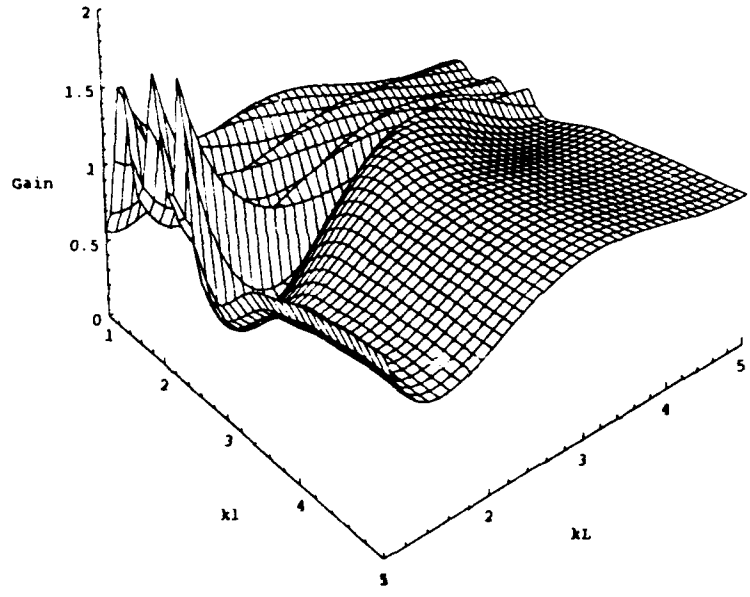

(a)

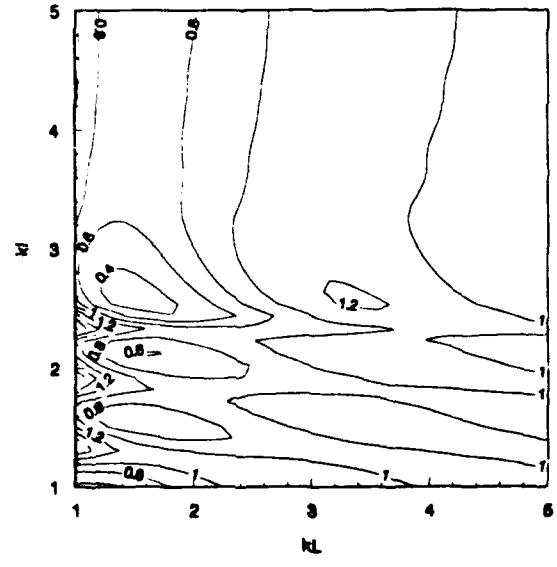

(b)

Figure 4-2 Gain in radiation resistance versus *kL* and *kl* for the line configuration type I with six resonators at 1 atm ambient pressure (a) 3D surface plot (b) contour plot

of acceptable values of ka, i.e. which yield a gain greater than a certain value, would be greater.

Tables 4-1 and 4-2 present results for the line configuration type I for one through fourteen resonators at 1 atm ambient pressure and with $ka_r=0.1$ respectively. Notice that the gain remains fairly constant at about 1.2. The relative volume velocities listed are those for the resonator closest to the transducer. As before, the primary difference between the two tables is the values of ka. It can be shown that the ratio ka/ka_r is the same for both.

C. BEAM PATTERNS AND DIRECTIVITY

Figure 4-3 shows the three-dimensional far-field beam pattern for the line type I configuration with six resonators at 1 atm ambient pressure. The acoustic axis is along the negative x-axis. Figure 4-4 shows a polar plot of the beam pattern. The directivity index, found from Figure 4-4 or Table 4-1, is 4.6. The line configuration type I can be used to increase the power output and directivity of an underwater transducer; however, the conical configuration results are clearly better.

In the last section, we described divergent peaks in the plot of gain in radiation resistance for vanishing kL. For one of these peaks, for example, the gain at $kL=1$ and $kl=2.33$ is 1.82. We plotted a beam pattern using these values in order to better understand these peaks in the gain plot. The directivity index was found to be $DI=11.0$. Figure 4-5 is a polar plot of the resulting beam pattern. The acoustic axis is now the positive x-axis. This is an indication that the peaks as kL goes to zero correspond to a

N	ka	kl	kL	$Gain$	$\mid U^{rel} \mid$	$\angle U^{rel}$	DI
1	0.0138101	----	2.80	1.11	0.330	90.0	0.8
2	0.0137779	2.09	3.08	1.16	0.437	86.2	1.9
4	0.0137538	2.32	3.34	1.20	0.511	86.1	3.7
6	0.0137347	2.49	3.59	1.22	0.503	86.0	4.6
8	0.0137216	2.62	3.68	1.22	0.472	87.3	5.2
10	0.0137276	2.60	3.56	1.24	0.518	86.6	5.4
12	0.0137201	2.64	3.59	1.24	0.510	90.5	5.5
14	0.0138101	2.67	3.61	1.25	0.505	91.1	5.5

Table 4-1 Line configuration type I results for air bubbles at 1 atm ambient pressure.

N	ka	kl	kL	$Gain$	$\mid U^{rel} \mid$	$\angle U^{rel}$	DI
1	0.102413	------	2.80	1.11	0.331	90.0	0.8
2	0.100606	2.09	3.08	1.16	0.439	86.2	2.0
4	0.0993406	2.32	3.34	1.20	0.514	86.1	3.7
6	0.0987282	2.45	3.46	1.22	0.530	87.3	4.6
8	0.0983271	2.53	3.52	1.23	0.528	88.5	5.1
10	0.0980380	2.60	3.57	1.24	0.522	89.6	5.4
12	0.0978263	2.64	3.59	1.24	0.514	90.5	5.5
14	0.0978263	2.67	3.61	1.25	0.509	91.0	5.5

Table 4-2 Line configuration type I results for resonators with $ka_r=0.1$.

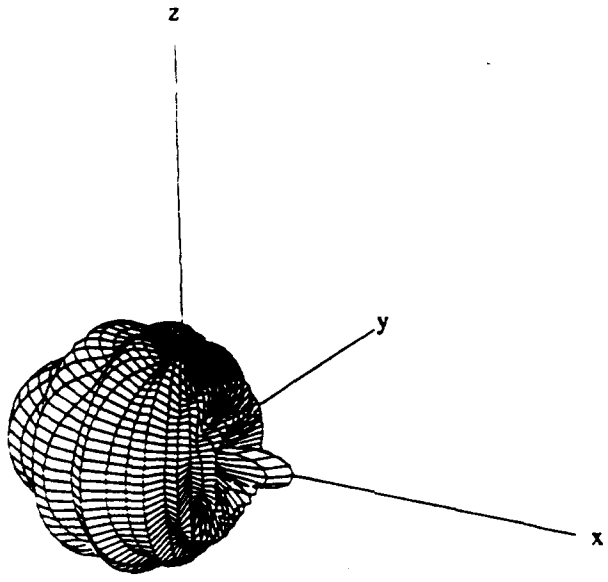

Figure 4-3 Three-dimensional beam pattern for the line configuration type I with six resonators at 1 atm ambient pressure.

condition on the values of *kl* that provide constructive interference. It is probably related to the total length of the aperture. Further investigation is required to fully understand the occurence of these gain peaks and to determine whether a practical system can utilize this phenomenon. If exploitable, this system provides the best directivity of any analyzed in this research.

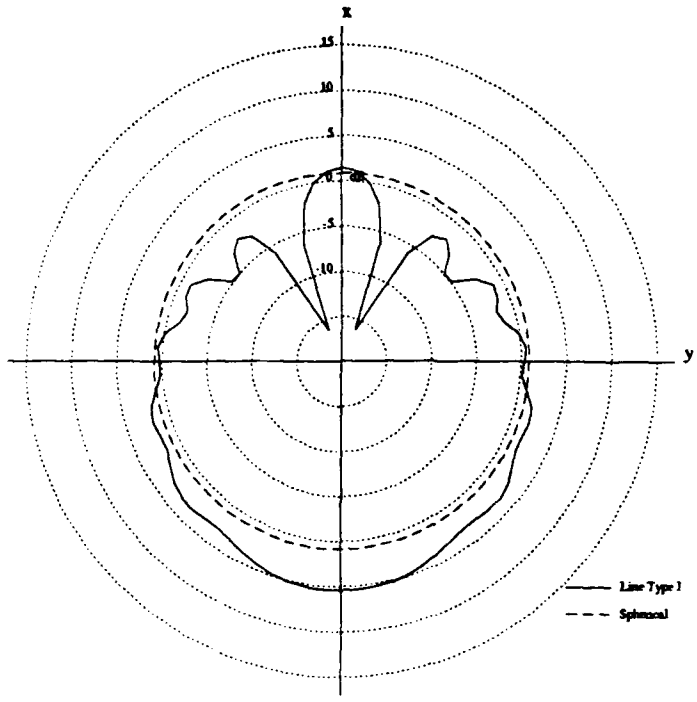

Figure 4-4 Polar plot of the beam pattern for the line configuration type I with six resonators at 1 atm ambient pressure

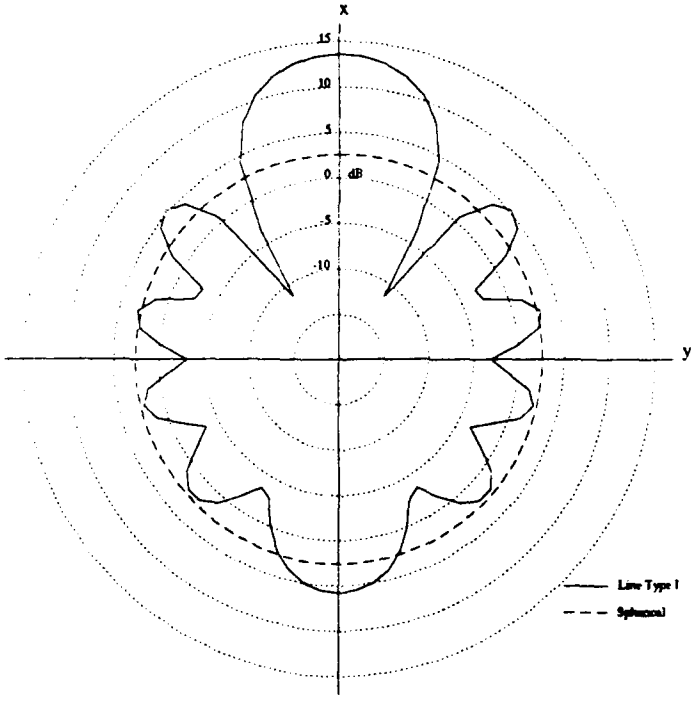

Figure 4-5 Polar plot of the beam pattern for the line configuration type I with six resonators at 1 atm ambient pressure for the divergent peak. kL=1, kl=2.33

V. LINE CONFIGURATION TYPE II

A. THE GEOMETRY

Figure 5-1 shows the geometry for the line configuration type II with six resonators. In this configuration, half of the resonators are on one side of the transducer and half are on the other side. The dimensionless distance from the transducer to thefirst resonator on either side is kL. The dimensionless inter-resonator spacing is kl. The transducer is assumed to have a dimensionless radius of ka_0=0.2.

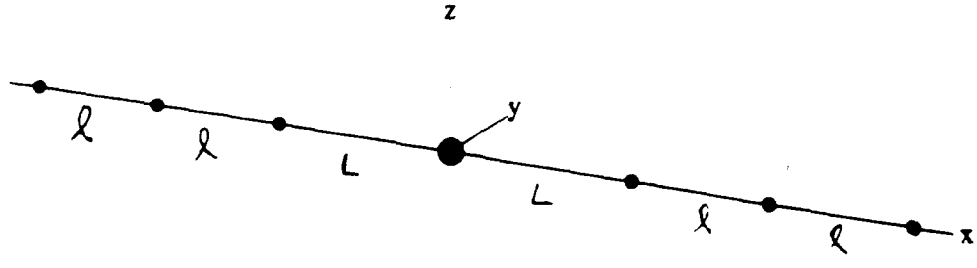

Figure 5-1 Geometry of the line configuration type II with six passive acoustic resonators.

B. GAIN IN RADIATION RESISTANCE

The gain in radiation resistance versus kL and kl for a fixed ka is shown in Figure 5-2. The value chosen for ka is the value that provides maximum gain at the local maxima at kL=3.0 and kl=2.2, for which ka=0.01376. The gain at this point is 1.56. As with the line type I, the gain plot for line type II diverges as kL goes to zero. We have not investigated this behavior in detail. Tables 5-1 and 5-2 give the numerical results for line type II for two through twenty air bubbles at 1 atm ambient pressure and for resonators with ka_r=0.1 respectively.

N	*ka*	*kl*	*kL*	*Gain*	$\lvert U^{rel} \rvert$	$\angle U^{rel}$	*DI*
2	0.0138092	-----	2.65	1.26	0.386	90.0	0.7
4	0.0137761	2.06	2.87	1.42	0.631	84.3	2.7
6	0.0137595	2.24	2.99	1.56	0.752	84.9	2.8
8	0.0137478	2.38	3.06	1.68	0.852	85.0	4.9
10	0.0137387	2.48	3.10	1.78	0.923	85.4	5.5
12	0.0137315	2.54	3.17	1.88	0.979	85.1	5.9
14	0.0137247	2.62	3.15	1.96	1.014	86.4	6.1
16	0.0137192	2.67	3.16	2.04	1.046	86.9	6.3
18	0.0137143	2.70	3.17	2.10	1.073	87.3	6.4
20	0.0137099	2.74	3.18	2.17	1.096	87.7	6.5

Table 5-1 Line configuration type II results for air bubbles at 1 atm ambient pressure.

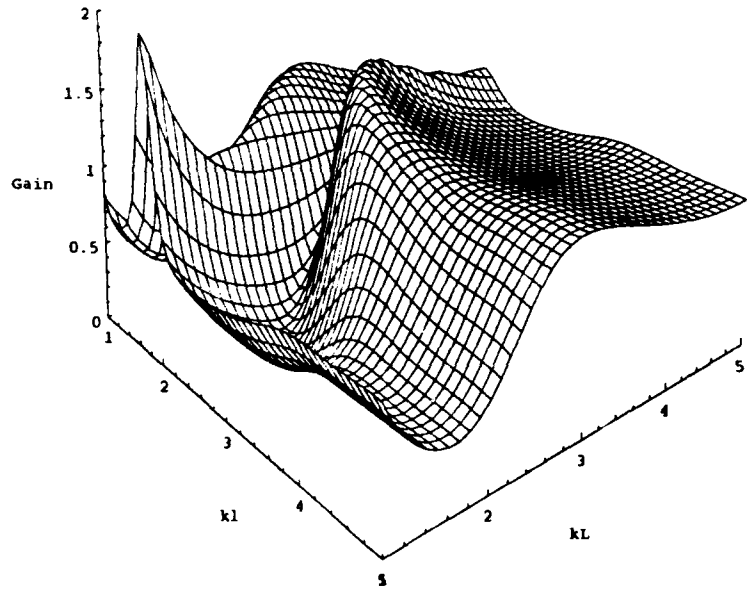

(a)

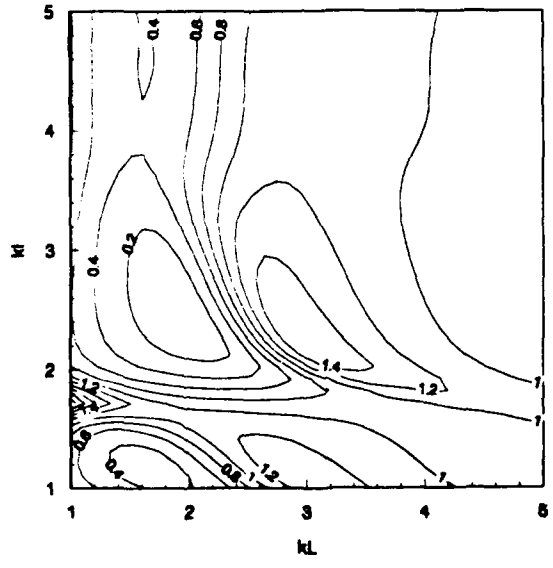

(b)

Figure 5-2 Gain in radiation resistance versus *kL* and *kl* for the line configuration type II with six resonators at 1 atm ambient pressure (a) 3D surface plot (b) contour plot

As seen in Table 5-1, the gain in radiation resistance does not reach a constant value (over the range of N considered). For twenty resonators the gain is 2.17. This is the highest gain calculated in this research. The values of kl and kL are the same in Tables 5-1 and 5-2. The difference is in the values of ka. It can be shown that the ratio ka/ka_r is the same in both cases.

N	ka	kl	kL	*Gain*	$\lvert U^{rel} \rvert$	$\angle U^{rel}$	*DI*
2	0.102360	-----	2.65	1.26	0.388	90.0	0.7
4	0.100526	1.89	2.98	1.42	0.633	84.2	2.9
6	0.0996309	2.24	2.99	1.56	0.756	84.9	4.1
8	0.0990346	2.38	3.06	1.68	0.857	85.1	5.0
10	0.0985781	2.48	3.10	1.78	0.927	85.5	5.5
12	0.0982567	2.53	3.20	1.87	0.992	84.7	5.9
14	0.0978998	2.62	3.15	1.96	1.02	86.4	6.1
16	0.0976349	2.66	3.16	2.04	1.05	86.9	6.3
18	0.0974038	2.70	3.17	2.11	1.08	87.3	6.4
20	0.0971994	2.74	3.18	2.17	1.10	87.6	6.5

Table 5-2 Line configuration type II results for resonator with ka_r=0.1.

C. BEAM PATTERNS AND DIRECTIVITY

Figure 5-3 shows the three-dimensional far-field beam pattern for the line configuration type II with six resonators at 1 atm ambient pressure. The beam pattern for this configuration is not particularily interesting. The acoustic axis is along the

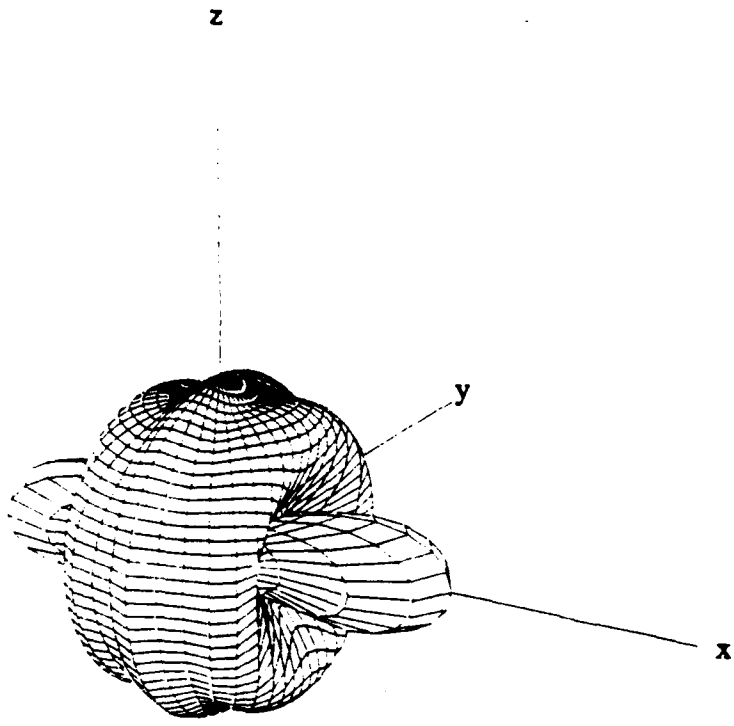

Figure 5-3 Three-dimensional beam pattern for the line configuration type II with six resonators at 1 atm ambient pressure.

positive and negative axes and there is some directivity. Figure 5-4 shows the dB beam pattern. The directivity index (*DI*), from Figure 5-4 or Table 5-1, is 4.9 dB. Unlike the circular configurations, the *DI* does not reach a constant valve (over the range of *N* considered). For twenty resonators, the line type II provides a directivity index of 6.5 dB.

Figure 5-5 shows the beam pattern for this configuration when using the value of *kl* corresponding to the peak at $kL=1$. The value of *kl* is 1.72, the directivity index is 8.0 dB, and the gain is 2.15. The large gain and high directivity makes this system

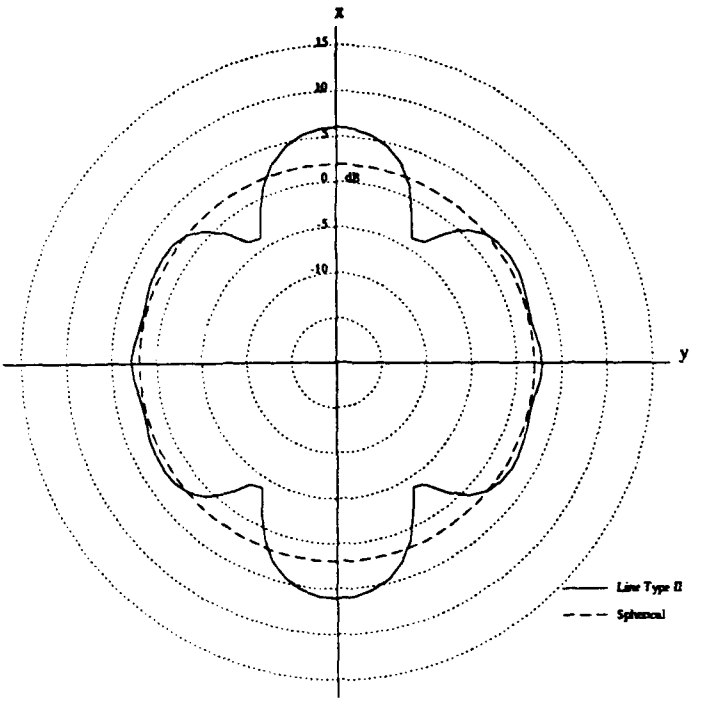

Figure 5-4 Polar plot of the beam pattern for the line configuration type II with six resonators at 1 atm ambient pressure

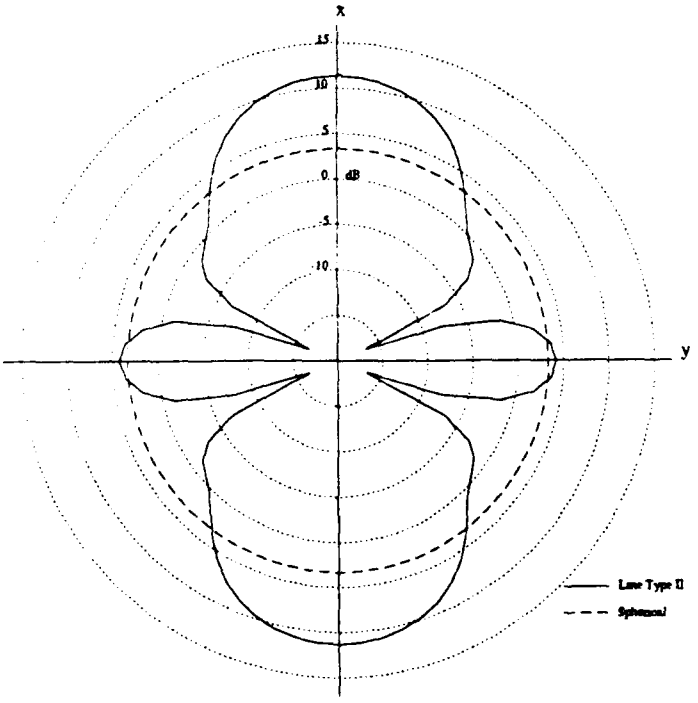

Figure 5-5 Polar plot of the beam pattern for the line configuration type II with six resonators at 1 atm ambient pressure for the divergent peak. kL=1, kl=1.72

potentially useful for practical application. However, further investigation is required to understand this behavior and to determine whether a practical system can utilize the large gain in radiation resistance at small values of kL. We provide the result as a basis for this investigation.

VI. AN ACOUSTIC YAGI-UDA ARRAY

The Yagi-Uda electomagnetic antenna system [Ref. 5] uses parasitic antenna elements around a feed antenna element in order to direct a travelling wave. It depends on mutual coupling between the elements. The analogy to the underwater transducer with passive acoustic resonators is direct. The transducer is the feed element and the passive acoustic resonators are the parasitic elements. In the underwater case, the elements are coupled by the sound field. We are basically trying to do the same thing that antenna farm designers have been doing for years with radio waves. Once you get past the obvious analogy, the similarities end. The acoustic Yagi-Uda array described here is more closely related to the work described earlier in this paper than to the electromagnetic antenna system. We will alternately refer to the Yagi-Uda array as line configuration type III. In the sections that follow, we will develop the theory and then present numerical and graphical results.

A. THEORY

In the design of the Yagi-Uda configuration (line type III), we are interested in directing the sound energy by choosing resonators that will produce constructive interference in one direction and destructive interference in the opposite direction. We also impose the condition that the gain in radiation resistance be not less than one.

For constructive interference, we require that the phase of the pressure wave outgoing from a resonator equal the phase of the pressure wave incident at the resonator from the transducer. This constraint can be met only if the resonator is stiffness controlled. We then place an additional constraint on the system requiring that the gain be one or greater. For this condition, we must have the phase of the pressure wave incident at the transducer from a resonator equal to the phase of the pressure wave outgoing from the transducer. These two constraints require (1) the resonators must be stiffness-controlled, and (2) the dimensionless distance from the transducer must satisfy

$$kd_m = m\pi , \qquad m=1,2,3,... \tag{6-1}$$

where d_m = the distance from each resonator to the transducer

and k = wavenumber in the medium.

For destructive interference, we require that the phase of the pressure wave outgoing from a resonator equal π plus the phase of the pressure wave incident at the resonator from the transducer. This constraint can only be met if the resonator is mass-controlled. We then use the constraint that the gain be one or greater. These two contraints require (1) the resonators must be mass-controlled, and (2) the dimensionless distance from the transducer must satisfy

$$kd_m = \frac{\pi}{2} + m\pi , \qquad m=1,2,3,... \tag{6-2}$$

We force the resonators to be approximately stiffness-controlled yet still close to resonance by setting $ka = ka_r - 1/2(ka_r)^2$. We force the resonators to be approximately

mass-controlled and likewise close to resonance by setting $ka = ka_r + 1/2(ka_r)^2$. These values result in the resonators being driven at a frequency which is one resonant half-width above and below their resonant frequency (the resonant half-width is $1/2(ka_r)^2$).

Figure 6-1 is a diagram of the line type III configuration. We show the distances

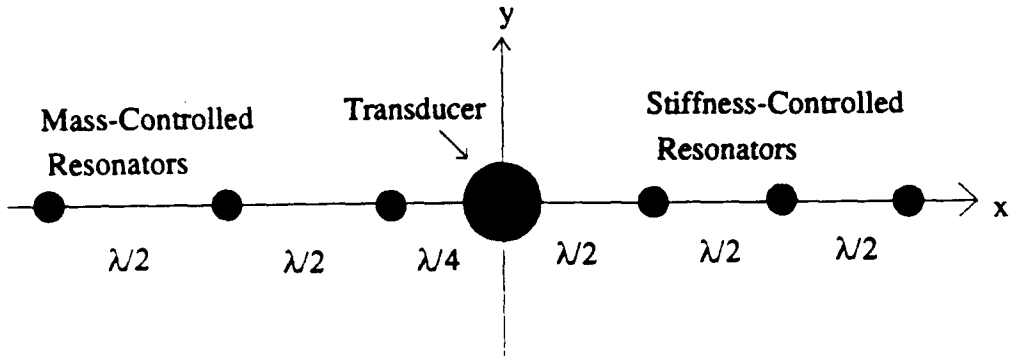

Figure 6-1 Diagram of the Yagi-Uda configuration (line type III) for six resonators.

in terms of wavelengths and indicate which resonators are mass- and stiffness- controlled. In the next section we present the results of this research.

B. RESULTS

Computer simulations of the line type III configuration indicate that the analysis of the theory in the previous section is correct. We did not perform any optimization of parameters on this configuration as we did for previous configurations. The results presented here are for the distances and radii described in the previous section.

Figure 6-2 shows a three-dimensional far-field beam pattern for a line type III configuration of six resonators. The acoustic axis is along the positive x-axis, as expected. Figure 6-3 shows the polar plot of the beam pattern. Table 6-1 lists the gain

N	*Gain*	*DI*
2	0.83	4.9
4	0.90	5.9
6	0.94	6.4
8	0.97	6.5
10	0.99	6.5

Table 6-1 Results for the Yagi-Uda configuration (line type III)

in radiation resistance and directivity index for two through ten resonators. The gain for six or more resonators is about one and the directivity index is about 6.5 dB. Figure 6-4 is the beam pattern and Figure 6-5 the polar plot for the case of ten passive acoustic radiators, and is provided for comparison. As indicated in Table 6-1, there is no major difference in either the gain in radiation resistance or the directivity index for the N=6 and N=10 cases.

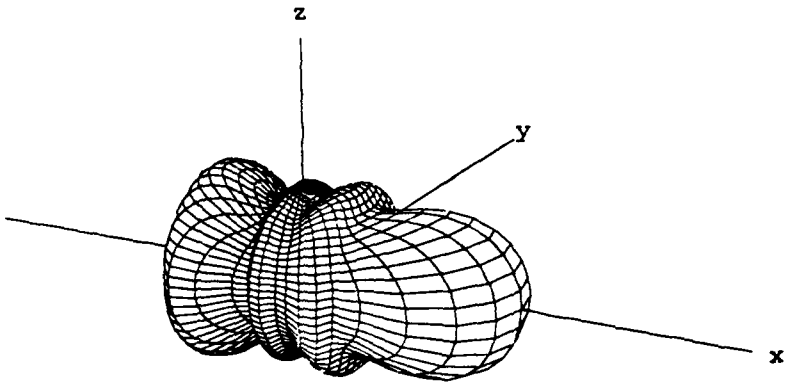

Figure 6-2 Three-dimensional beam pattern for line type III configuration with six resonators

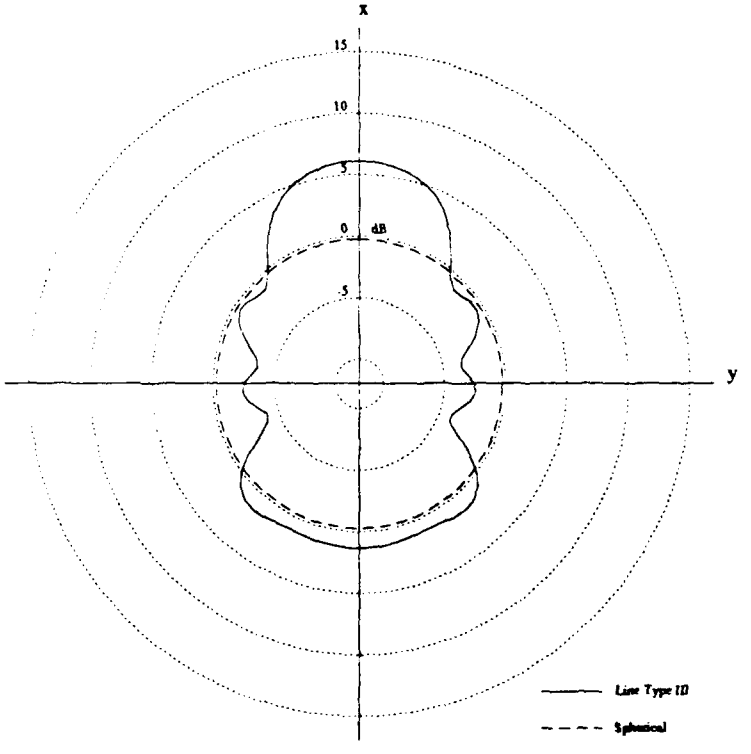

Figure 6-3 Polar plot of the beam pattern for the line type III configuration with six resonators

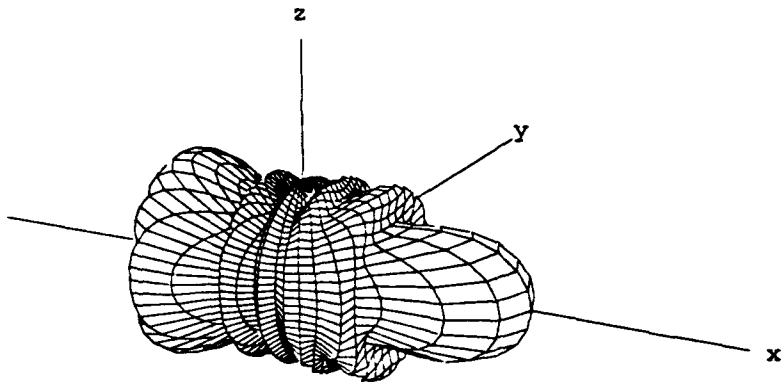

Figure 6-4 Three-dimensional beam pattern for line type III configuration with ten resonators

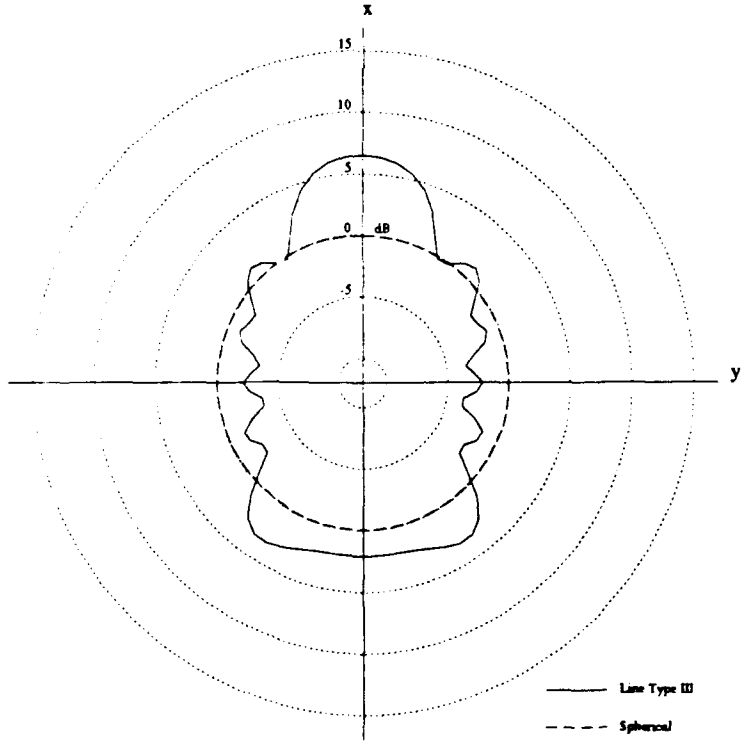

Figure 6-5 Polar plot of the beam pattern for the line type III configuration with ten resonators

VII. DISCUSSION

We have analyzed five configurations of resonators and provided many graphs and tables of results. Table 7-1 is a comparison of the results for all configurations. The measures of effectiveness that we chose for comparison are (1) gain in radiation resistance, (2) directivity index, and (3) the far-field beam patterns. Table 7-1 lists the

N	Planar		Conical		Line Type I		Line Type II		Line Type III	
	Gain	*DI* dB	*Gain*	*DI* dB	*Gain*	*DI* dB	*Gain*	*DI* dB	*Gain*	*DI* dB
2	1.26	1.2	1.29	4.3	1.16	1.9	1.26	0.7	0.83	4.9
4	1.87	6.2	1.78	8.1	1.20	3.7	1.42	2.7	0.90	5.9
6	1.95	6.7	1.82	8.4	1.22	4.6	1.56	2.8	0.94	6.4
8	1.95	6.7	1.82	8.4	1.22	5.2	1.68	4.9	0.97	6.5
10	1.96	6.7	1.82	8.4	1.24	5.4	1.78	5.5	0.99	6.5

Table 7-1 Comparison of the results for all configurations

data for the first two measures of effectiveness and Figure 7-1 provides a comparison of the far-field beam patterns on a single plot. Recall that 0 dB represents the transducer with no resonators present. We considered the case of six resonators throughout the investigation as a basis for comparison of the three-dimensional beam patterns. The N=6 case is highlighted in Table 7-1. The planar configuration has the best gain, almost double, and the conical configuration has the best directivity index, 8.4 dB. Figure 7-1

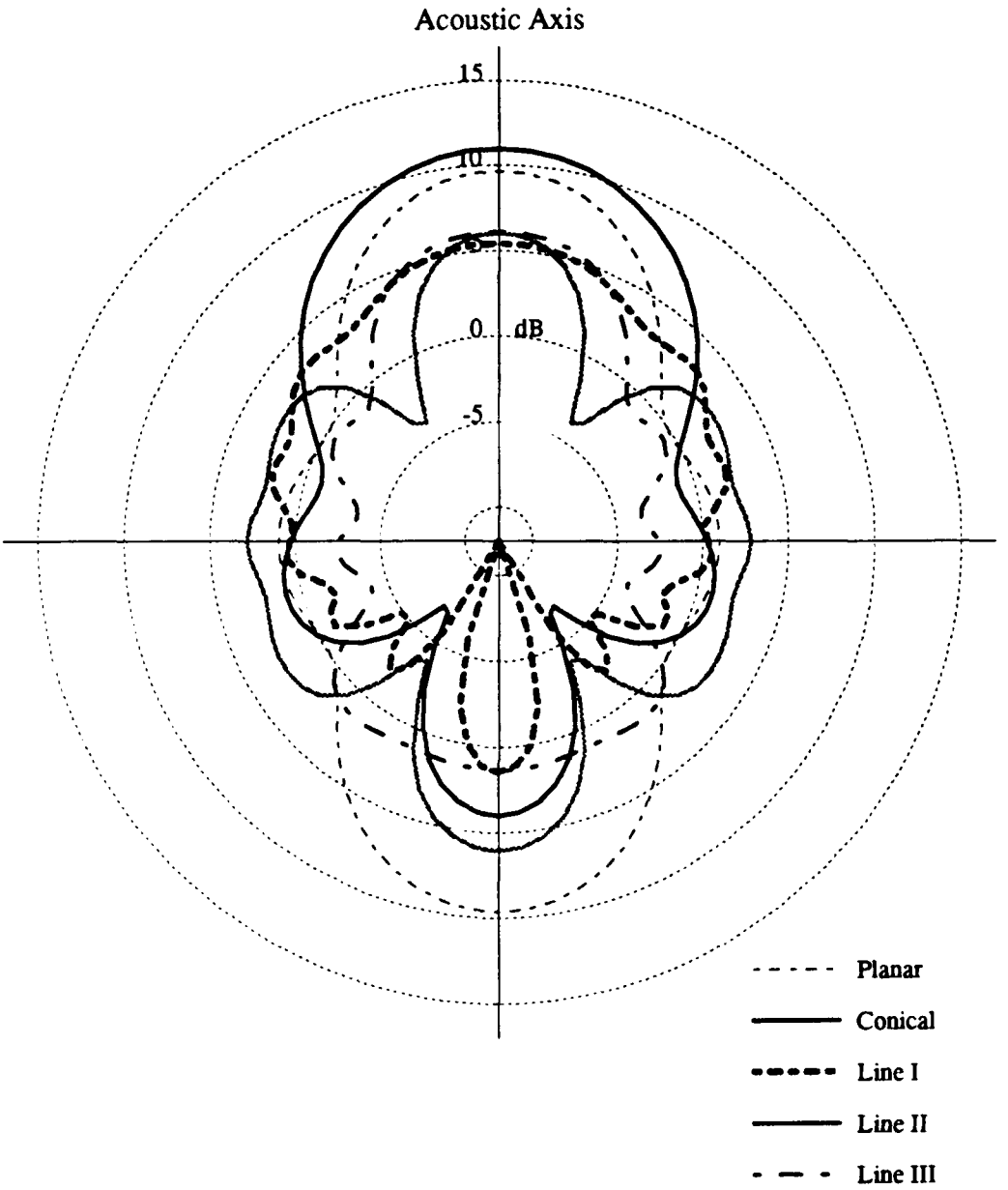

Figure 7-1 Polar plot of the far-field beam pattern for all configurations for six resonators.

shows that the conical configuration also has the best front-to-back discrimination along the acoustic axis. Of the results presented, clearly the conical configuration is the best choice for a real system. The linear configurations are generally worse than the circular configurations, but the line type III configuration is of particular interest. The addition of six passive acoustic resonators in a Yagi-Uda antenna-like configuration greatly improves the directivity of the transducer. However, since the passive resonators are not driven at their resonant frequency, this configuration does not provide any power gain.

Further investigation of the divergent peaks in gain for the line configurations type I and II is warranted. The gain diverges as the distance, L, to the first resonator tends toward zero. It may be possible to exploit regions of finite kL for which this behavior occurs. Certain values of resonator spacing satisfy a resonant condition related to the total length of the aperture which apparently results in substantial gain. We presented beam patterns for a system operating on one of these divergent gain peaks and found that the directivity and gain of the system were better than any other system analyzed. Further investigation into this behavior is encouraged.

We have shown that resonators with a value of $ka_r = 0.1$ provide identical results in terms of gain and directivity as do bubbles at 1 atm ambient pressure. We also demonstrated that these resonators are not as sensitive to the value of ka, that is, substantial gain (≥ 1.5) may be achieved over a reasonable range of operating frequencies. This is understood as follows. For an air-filled bubble at 1 atm ambient pressure, $Q = 1/ka_r$ is about 70. For a system to be feasible, the dimensions of each resonator must be matched to substantially better than one part in Q. It is probably not

reasonable to expect that a collection of bubbles can be matched closely enough in radius for a system at 1 atm ambient pressure to be practical. It may be possible to build, however, a system of bubble-like resonators such as thin-walled shells that will have a ka_r of about 0.1 and therefore a Q of about 10.

Table 7-2 describes the physical size of a system for various configurations of six resonators as described in this thesis. The overall dimensions of the system are the same

Frequency:	10 Hz		100 Hz		1 kHz	
Radius of (cm): Resonator	33	240	3.3	24	0.33	2.4
Aperture size of (m): Planar	137		13.7		1.37	
Conical	128		12.8		1.28	
Line Type I	383		38.3		3.83	
Line Type II	357		35.7		3.57	
Line Type III	413		41.3		4.13	

Table 7-2 Physical size of the system of resonators for 10 Hz, 100 Hz, and 1 kHz for various configurations of six resonators.

for bubbles at 1 atm ambient pressure and for ka_r=0.1 resonators. The size of the resonator increases for larger values of ka_r. The conical configuration, chosen as the best in terms gain and directivity, has the smallest physical dimensions. The aperture size (diameter for circular and total length for linear configurations) for the conical

configuration at 100Hz is about 13 meters. A $ka_r = 0.1$ resonator for this case would have a radius of 24 cm.

VIII. CONCLUSION

A. SUMMARY

We developed the equations for the network analysis of a transducer in the presence of passive acoustic radiators. These equations were implemented in computer programs and applied to five configurations of resonators. We first considered the two configurations previously examined by Ellsworth. We provided results for the case of six resonators and developed three-dimensional beam patterns. We then examined two linear configurations and provided results. Next, we developed the idea of a Yagi-Uda antenna-like array of passive acoustic resonators. Finally, we conducted a comparison of all five configurations.

B. CONCLUSIONS

We found that the conical configuration of six resonators is the best choice in terms of the gain in radiated power output, directivity along an acoustic axis, and minimum required number of resonators. A linear configuration could be utilized to improve the gain and directivity of a transducer, but not as well as the conical configuration. We found that the acoustic Yagi-Uda antenna configuration can be used to improve the directivity of an underwater transducer.

C. RECOMMENDATIONS

The results of the research presented in this paper are promising. We recommend that further work be done to (1) design a resonator with $ka_r = 0.1$, (2) build a system of resonators and verify the theory and results in this paper, (3) study the Yagi-Uda configuration in more detail including optimizations to improve the gain , and (4) study the divergent peaks in gain as kL goes to zero for the linear configurations to determine whether a practical system can be designed to utilize the higher theoretical gain and directivity.

APPENDIX

The following Mathematica program code is an example of how programs were written to perform the calculations in this paper. The example consists of the standard definitions for the conical configuration and code to create plots as found in this document and calculate the information found in tables for the conical configuration. The lines in bold face type are comments.

Distance, Radius, and Area

```
ClearAll[ka,S,kl,krange]
ka[0] := ka0
ka[n_] := kai
S[n_] := ka[n] ^ 2
kl[n_,n_] := 0
kl[n_,0] := Sqrt[kR^2 + kH^2]
kl[0,n_] := Sqrt[kR^2 + kH^2]
kl[n_,m_] := kR Sqrt[2-2*Cos[(2 Pi/Num) (n-m)]]
krange[0,the_,ph_] := kr
krange[n_,the_,ph_] := Sqrt[
    (kr Sin[the] Cos[ph] - kR Cos[(2 Pi n)/Num])^2 +
    (kr Sin[the] Sin[ph] - kR Sin[(2 Pi n)/Num])^2 +
    (kr Cos[the] - kH)^2]
```

Impedances

```
ClearAll[Za,Zar,Dfc]
Dfc[n_] := Exp[j ka[n]] / (1+ka[n])
Za[n_] := - I (S[0]/S[n]) ((3 gam Po)/(p c^2 ka[n]))
Zar[n_,n_] := (S[0]/S[n]) (I ka[n]/(1+I ka[n]))
Zar[n_,m_] := Dfc[n] Zar[m,m] (ka[m]/kl[n,m]) Exp[
                    I (ka[m] - kl[n,m])]
```

Gain in radiation resistance

```
ClearAll[ZB,ZC,Gain]
ZB[n_] := Zar[n,0]
ZC[n_,n_] := Zar[n,n] + Za[n]
ZC[n_,m_] := Zar[n,m]
Gain := Re[Zar[0,0] - Array[ZB,Num] . Inverse[Array[
        ZC,{Num,Num}]] . Array[ZB,Num]]/Re[Zar[0,0]]
```

Relative velocities and field pressure

```
Clear[theta,phi,the,ph,n]
ClearAll[BP,dBBP,Prad,Urel]
Urel := - Inverse[Array[ZC,{Num,Num}]] . Array[ZB,Num];
Prad[0,the_,ph_] := Zar[0,0] (ka[0]/krange[0,the,ph]) Exp[
       I (ka[0]-krange[0,the,ph])]
Prad[n_,the_,ph_] := Zar[n,n] Urel[[n]] (ka[n]/
       krange[n,the,ph]) Exp[I (ka[n]-krange[n,the,ph])]
BP[the_,ph_] := Abs[Sum[Prad[n,the,ph],{n,0,Num}]]/
              Abs[Prad[0,the,ph]]
dBBP[the_,ph_] := 20 Log[10,BP[the,ph]]
```

Constants

```
Clear[kH,kai,ka0,kR,kr,kar,gam,Po,c,p]
gam=1.402;
Po=1.013 10^5;
c=1500;
p=998;
kar=Sqrt[(3 gam Po)/(p c^2)]
Num=6
kH=Pi/2
ka0=0.2
```

Create surface plot of Gain versus *ka* and *kR*

```
plot1=Plot3D[Gain,{kR,1,5},{kai,0.9 kar,1.1 kar},
            PlotPoints->40,PlotRange->{0,2},
            AxesLabel->{"kR","ka","Gain"}]
```

Create contour plot

```
plot2=Show[ContourGraphics[plot1],
      Frame->True,
      FrameLabel->{"kR","ka"},
      RotateLabel->True,
      ContourSmoothing->3,
      ContourShading->False,
      AspectRatio->1,
      Contours->{0.2,0.4,0.6,0.8,1.0,1.2,1.4,1.6,1.8}]
```

Find Maximum Gain

```
Clear[kai,kR]
{maxgain,{kaiRule,kRrule}}=
        FindMinimum[-Gain,{kai,{kar,1.002 kar}},
                    {kR,{2.7,2.8}}]
kai=kai/.kaiRule
kR=kR/.kRrule
MaxGain=-maxgain
```

Find relative volume velocities

```
N[{Abs[Urel[[1]]],Arg[Urel[[1]]] 180/Pi}]
```

Find directivity index

```
thAxis = 0;        (* theta on acoustic axis *)
phAxis = 0;        (* phi on acoustic axis   *)
DI = dBBP[thAxis,phAxis] -
        20 Log[10,Sqrt[MaxGain]] //N
```

Create 3D beam pattern

```
BP2[th_,ph_]=Evaluate[BP[th,ph]];
Needs["Graphics`ParametricPlot3D`"]
plot3=ParametricPlot3D[BP2[theta,phi]
                  {Sin[theta] Cos[phi],
                   Sin[theta] Sin[phi],
                   Cos[theta]},
                  {theta,0, Pi, Pi/40},
                   phi,0, 2 Pi, Pi/20}]
```

Create 2D (dB) beam pattern in z-x plane

```
data=Table[N[dBBP[theta,0]],
            {theta,0,2 Pi,Pi/40}];
mystuff=Table[(data[[i]] + 12)
      {N[Sin[(i-1) Pi/40]],N[Cos[(i-1) Pi/40]]},
      {i,1,81}];
myplot=ListPlot[mystuff,PlotJoined->True,
AspectRatio->Automatic]
```

The following requires a separately created template and label:

```
Show[template,label,myplot,
     AspectRatio->Automatic,
     Axes->False,PlotRange->All]
```

REFERENCES

[1] Tolstoy, I. "Superresonant systems of scatterers. I," *Journal of the Acoustical Society of America*, **80**(1), pp.282-294, 1986.

[2] Tolstoy, A. and Tolstoy, A. "Superresonant systems of scatterers. II," *Journal of the Acoustical Society of America*, **83**(6), pp 2086-2096, 1988.

[3] Tolstoy, I. "Line and plane arrays of resonant monopole scatterers," *Journal of the Acoustical Society of America*, **87**(3), pp 1038-1043, 1990.

[4] Ellsworth, J. "On The Use of Sympathetic Resonators to Improve Low Frequency Sonar Performance," Naval Postgraduate School Thesis, September 1990.

[5] Milligan, T. *Modern Antenna Design*, McGraw-Hill, New York, 1985.

[6] Wolfram, S. *Mathematica: A System For Doing Mathematics By Computer*, 2nd edition, Addison-Wesley, Redwood City, CA, 1991.

[7] Bobber, R. *Underwater Electroacoustic Measurements*, Peninsula Publishing, Los Altos, CA, 1988.

[8] Kinsler, L., Frey, A., Coppens, A., Sanders, J. *Fundamentals of Acoustics*, 3rd edition, Wiley, New York, 1982.

[9] Clay, C., Medwin, H. *Acoustical Oceanography*, Wiley, New York, 1977.

INITIAL DISTRIBUTION LIST

		No. Copies
1.	Defense Technical Information Center Cameron Station Alexandria, VA 22304-6145	2
2.	Library, Code 52 Naval Postgraduate School Monterey, CA 93943-5002	2
3.	Physics Department Naval Postgraduate School ATTN: Professor S.R. Baker (Code PH/BA) Monterey, CA 93943-5000	2
4.	Physics Department Naval Postgraduate School ATTN: Professor O.B. Wilson (Code PH/WL) Monterey, CA 93943-5000	1
5.	Physics Department Naval Postgraduate School ATTN: Professor A.A. Atchley (Code PH/AY) Monterey, CA 93943-5000	1
6.	Commanding Officer Naval Ocean Systems Center ATTN: Mr. Ed Rynne (Code 711) San Diego, CA 92152-5000	1
7.	Commanding Officer Naval Ocean Systems Center ATTN: Mr. Cliff Meland (Code 712) San Diego, CA 92152-5000	1

8. Commanding Officer — 1
Naval Research Lab - USRD
ATTN: Dr. A. Lee Van Buren (Code 5980)
Orlando, FL 32856

9. Commanding Officer — 1
Naval Research Lab - USRD
ATTN: Dr. Robert Timme (Code 5970)
Orlando, FL 32856

10. Commanding Officer — 1
Naval Underwater Systems Center
ATTN: Mr. Bernard McTaggart (Code 213)
New London, CT 06320-5594

11. Commanding Officer — 1
Naval Underwater Systems Center
ATTN: Dr. Roger Richards (Code 2131)
New London, CT 06320-5594

12. Commanding Officer — 1
Pearl Harbor Naval Shipyard
ATTN: LT D. E. Sanders
Box 400
Pearl Harbor, HI 96860-5350